Journal of Medicinal Chemistry

Article

Discovery of new chemical entities for old targets: insights on the lead optimization of chromone-based monoamine oxidase B (MAO-B) inhibitors

Joana Reis, Fernando Cagide, Daniel Chavarria, Tiago B. Silva, Carlos Fernandes, Alexandra Gaspar, Eugenio Uriarte, Fernando Remião, Stefano Alcaro, Francesco Ortuso, and Fernanda M. Borges

J. Med. Chem., **Just Accepted Manuscript** • DOI: 10.1021/acs.jmedchem.6b00527 • Publication Date (Web): 31 May 2016

ACS Publications

Journal of Medicinal Chemistry is published by the American Chemical Society. 1155 Sixteenth Street N.W., Washington, DC 20036

Discovery of new chemical entities for old targets: insights on the lead optimization of chromone-based monoamine oxidase B (MAO-B) inhibitors

Joana Reis[a] ¥, Fernando Cagide[a] ¥, Daniel Chavarria[a], Tiago Silva[a], Carlos Fernandes[a], Alexandra Gaspar[a], Eugenio Uriarte[b], Fernando Remião[c], Stefano Alcaro[d], Francesco Ortuso[d] ¥, Fernanda Borges*[a]

[a]CIQUP/Department of Chemistry and Biochemistry, Faculty of Sciences, University of Porto, 4169-007, Porto, Portugal.

[b]Department of Organic Chemistry, Faculty of Pharmacy, University of Santiago de Compostela, 15782 Santiago de Compostela, Spain

[c]UCIBIO-REQUIMTE, Laboratory of Toxicology, Department of Biological Sciences, Faculty of Pharmacy, University of Porto, 4050-313, Porto, Portugal

[d]Department of "Scienze della Vita", University "Magna Græcia" of Catanzaro, 88100 Catanzaro, Italy

ABSTRACT

The discovery of new chemical entities endowed with potent, selective and reversible monoamine oxidase-B inhibitory activity is a clinically relevant subject. Therefore, a small library of chromone derivatives was synthesized and screened towards human monoamine oxidase isoforms (*h*MAO-A and *h*MAO-B). The structure-activity relationships studies strengthen the importance of the amide spacer and the direct linkage of carbonyl group to the γ-pyrone ring, along with the presence of *meta* and *para* substituents in the exocyclic ring. The most potent MAO-B inhibitors were *N*-(3'-chlorophenyl)-4-oxo-4*H*-chromene-3-carboxamide (**20**) (IC_{50} = 403 *p*M) and *N*-(3',4'-dimethylphenyl)-4-oxo-4*H*-chromene-3-carboxamide (**27**) (IC_{50} = 669 *p*M), acting as competitive and non-competitive reversible inhibitors, respectively. Computational docking studies provided insights into enzyme−inhibitor interactions and a rationale for the observed selectivity and potency. Compound **27** stands out due to its favorable toxicological profile and physicochemical properties, which pointed toward blood brain barrier permeability, thus being a valid candidate for subsequent animal studies.

Keywords: MAO-B inhibitors, New Chemical Entities, Chromone

INTRODUCTION

Parkinson's disease (PD) is one of the most prevalent neurodegenerative disorders, affecting up to 10 million people worldwide. Its current pharmacological therapy is mainly focused on improving the motor symptomatology and the patients' quality of life by slowing down the progression of symptoms and reducing morbidity. In spite of all the research performed in the field, there are only a few classes of drugs approved for the treatment of the motor related symptoms of PD, namely those acting primarily on the dopaminergic system, such as L-dopa, dopamine agonists, monoamine oxidase-B (MAO-B) and catechol-*O*-methyltransferase inhibitors.[1, 2]

Monoamine oxidases (MAOs) are intracellular flavine-containing enzymes that play a major role in the *in vivo* inactivation of biogenic amines, both in peripheral and central neuronal tissues. MAO-A and MAO-B are two isoforms of MAOs expressed in mammals, which can be distinguished based on their substrate preference and their interaction with specific inhibitors.[3-5] The primary substrates of MAOs in the human brain are neurotransmitters and, albeit dopamine can be metabolised by both isoforms, it has a higher affinity for MAO-B. The expression of MAO-B in neuronal tissues enhances 4-fold with aging, resulting in an increased level of dopamine metabolism and higher production of hydrogen peroxide, which are thought to play a relevant role in the aetiology of neurodegenerative diseases. Accordingly, the use of selective MAO-B inhibitors (IMAO-B), alone or combined with dopamine or its precursors, are important therapeutic approaches for neurodegenerative disorders, such as PD.[6]

Currently, there are two IMAO-B in the market: selegiline (R-(−)-deprenyl) and rasagiline which are selective but irreversible (Figure 1).[7] More recently, safinamide has been developed as a multi-target drug based on the enhancement of the dopaminergic function (through reversible inhibition of MAO-B and of dopamine reuptake) and

inhibition of the excessive release of glutamate in patients with early or mid- to late-stage PD (Figure 1).[8]

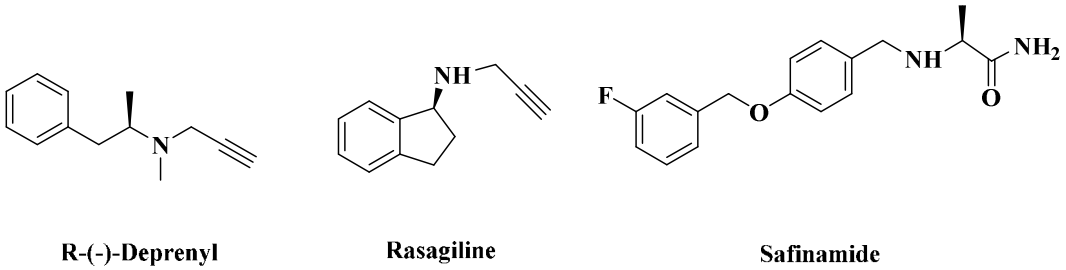

R-(-)-Deprenyl Rasagiline Safinamide

Figure 1. Structures of known MAO-B inhibitors.

However, due the lack of significant disease modifying properties, a pressing need for new chemical entities endowed with selective and reversible IMAO-B still exists. Chromones, a class of heterocyclic compounds widely distributed in nature, have attracted attention in the field of drug discovery and development due to their interesting biological activities.[9,10] Several lines of evidence reported by our research group have shown that chromone (4*H*-benzopyran-4-one) is a privileged structure for the rational discovery and development of new IMAO-B.[11-15] In this context, it was shown that the structural modification of the chromone scaffold with the insertion of a phenylcarboxamide moitey at position C3 of the γ-pyrone ring yielded selective IMAO-B.[11,14] Focusing on the lead optimization of chromone-3-phenylcarboxamide as IMAO-B and guided by the rational design strategy shown in Figure 2, the work herein reports the synthesis of a novel chromone library and the establishment of new structure-activity relationships (SAR). The evaluation of drug-like properties, kinetics and mechanism of enzymatic inhibition and cytotoxicity studies of the best chromone-based IMAO-B were also performed. Finally, in order to rationalize our results, docking

experiments were performed using models built on the basis of the crystal structures of human MAO-A and MAO-B.

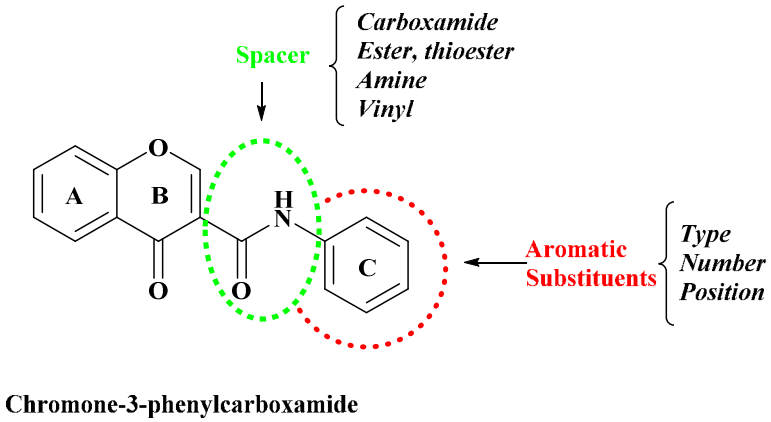

Figure 2. Structure of the lead compound described in previous work[14, 15] and rational design strategy followed for lead optimization.

RESULTS AND DISCUSSION

Chemistry. A lead optimization process of chromone-3-phenylcarboxamide was performed to improve its IMAO-B potency and selectivity. The rational design strategy described in Figure 2 was mainly focused on the study of: (i) the effect of different substituents (type, number and position) located on the aromatic exocyclic ring C and (ii) the importance of the amide linker located between the *γ*-pyrone nucleus (ring B) and the exocyclic aromatic ring (ring C) by the insertion of different spacers (amide, inverse amide, ester, thioester, amine and vinyl). As a result, a library of new chromone-based compounds was obtained (Schemes **1-3**). The first chromone series (Scheme **1**, compounds **2-31**) incorporated carboxamide, thioester or ester spacers directly attached to C-3 and an aromatic exocyclic ring with different electron donating or withdrawing substituents, variable in type, number and position. The chromone-based compounds were synthesized in moderate yields through a reaction that encompassed the *in situ*

generation of an acyl chloride intermediate, using phosphoryl chloride ($POCl_3$) in *N,N*-dimethylformamide (DMF), and the subsequent addition of the appropriate arylamine, 4-methylphenol or 4-methylbenzenethiol.[16] Compound **10** was obtained from compound **12** by cleavage of the *tert*-butoxycarbonyl protecting group with trifuoroacetic acid (TFA).

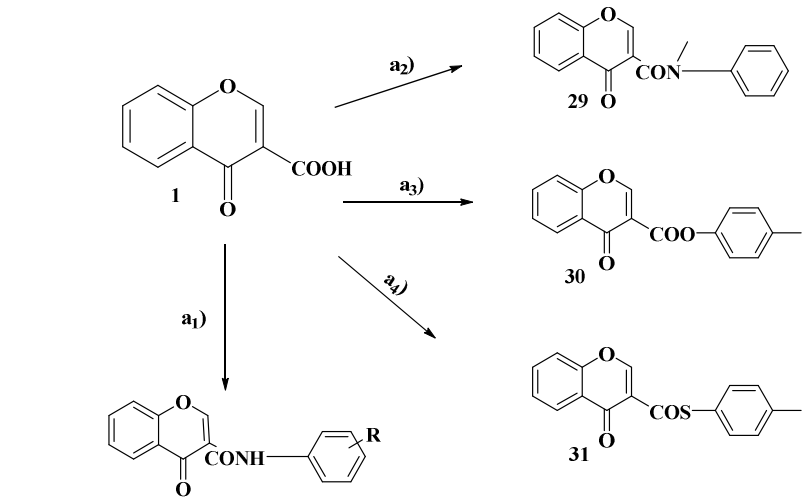

2 R=H	**15** R=4'-C_2H_5
3 R=4'-Cl	**16** R=2'-Cl-
4 R=4'-CH_3	**17** R=2'-Br
5 R=4'-OH	**18** R=2'-OH
6 R=4'-Br	**19** R=2'-CH_3
7 R=4'-I	**20** R=3'-Cl
8 R=4'-F	**21** R=3'-Br
9 R=4'-SH	**22** R=3'-OH
10 R=4'-NH_2	**23** R=3'CH_3
11 R=4'-$N(CH_3)_2$	**24** R=3',4'-Cl
12 R=4'-$NHCOOC(CH_3)_3$	**25** R=3',4',5'-Cl
13 R=4'-CCH	**26** R=2',3'-CH_3
14 R=4'-C_2H_3	**27** R=3',4'-CH_3
	28 R=3',4',5'-CH_3

b)

Scheme 1. General strategy followed for the synthesis of chromone-3-phenylcarboxamide derivatives (**2-31**) from chromone-3-carboxylic acid (**1**). Reagents and conditions: (a) $POCl_3$, DMF, appropriate arylamine (a_1), *N*-methylaniline (a_2), 4-methylphenol (a_3) or 4-methylbenzenethiol (a_4), r.t., 1-5h; (b) TFA, r.t., 2h.

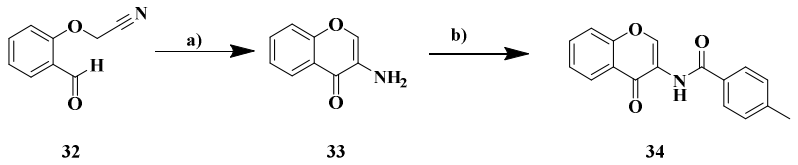

Scheme 2. Synthetic strategy followed for the synthesis of chromone derivative **34**. Reagents and conditions: (a) 5-(2-hydroxyethyl)-3,4-dimethylthiazolium iodide, DBU, r.t., 5h; (b) $POCl_3$, DMF, DIPEA, 4-methylbenzoic acid, r.t., 2h.

Compound **34,** bearing an inverted carboxamide linker at C-3, was obtained by a two-step synthetic strategy. Initially, an intramolecular cyclization between aldehyde and nitrile of compound **32** was performed in the presence of 5-(2-hydroxyethyl)-3,4-dimethylthiazolium iodide and 1,8-diazabicyclo[5.4.0]undec-7-ene (DBU), leading to the chromone amine **33** (Scheme **2**).[17] Subsequently, chromone **34** was synthesized by an *in situ* amidation reaction using 4-methylbenzoic acid, $POCl_3$ and DMF. In turn, compound **36** (Scheme **3**) was obtained by a reductive amination, in the presence of sodium triacetoxyborohydride, of the imine intermediate formed from the reaction of 3-formylchromone (**35**) with 4-methylaniline.[18]

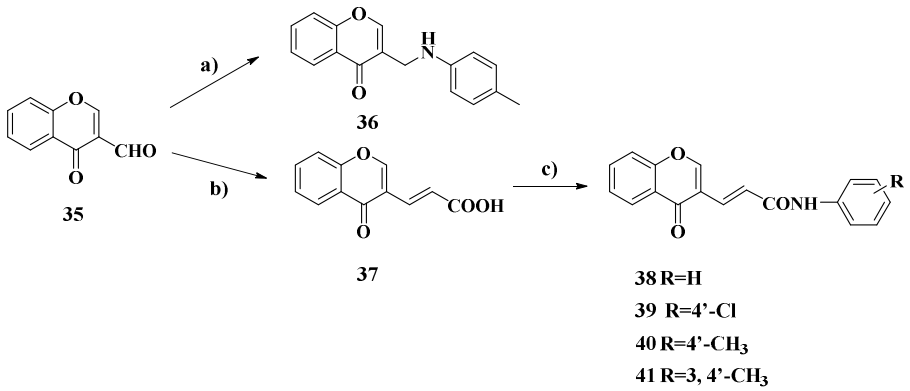

Scheme 3. Synthetic strategy followed for the synthesis of chromone derivatives (**36-41**) from 3-formylchromone (**35**). Reagents and conditions: (a) 4-methylaniline, $Na(AcO)_3BH$, r.t., 15 min; (b) malonic acid, pyridine, r.t., 1.5 h;(c) PyBOP, appropriate arylamine, DMF, DIPEA, r.t., 6h.

The synthetic procedure followed to obtain the chromone derivatives bearing a vinyl spacer linked to the γ-pyrone ring involved two steps (Scheme **3**). Firstly, the 3-(4-oxo-4*H*-chromen-3-yl)acrylic acid (compound **37**) was obtained from the reaction between 3-formylchromone (**35**) and malonic acid through a Knoevenagel-Doebner condensation.[19] The corresponding chromone carboxamides (compounds **38**-**41**) were then synthesized by a one-pot condensation reaction. Briefly, this amidation was performed using compound **37** and aniline or its ring-substituted derivatives as starting materials, using as coupling agent (benzotriazol-1-yloxy)-tripyrrolidinophosphonium hexafluorophosphate (PyBOP) in basic medium (*N,N*-diisopropylethylamine, DIPEA).[20]

Monoamine oxidase inhibition studies. The evaluation of *h*MAO inhibitory activity of the chromones under study was performed by a fluorescence-based assay measuring their effect on the production of hydrogen peroxide (H_2O_2) from *p*-tyramine (a common substrate for both *h*MAO-A and *h*MAO-B), using the Amplex Red MAO assay kit and microsomal MAO isoforms prepared from insect cells (BTI-TN-5B1-4) infected with recombinant baculovirus containing cDNA inserts for *h*MAO-A or *h*MAO-B.[14] The production of H_2O_2 catalyzed by MAO isoforms was detected using 10-acetyl-3,7-dihydroxyphenoxazine, a non-fluorescent and highly sensitive probe that reacts with H_2O_2 in the presence of horseradish peroxidase to produce a fluorescent product (resorufin).[14] The chromone derivatives under study and standard inhibitors did not react directly with the Amplex Red reagent, which indicated that they did not interfere with the measurements.

The results of the *in vitro* evaluation of inhibitory potency (IC_{50} values) and selectivity expressed as SI ([IC_{50} (MAO-A)]/[IC_{50} (MAO-B)]) towards *h*MAO-A and *h*MAO-B of

the chromones under study and standard inhibitors (clorgyline for MAO-A and (R)-(−)-deprenyl, rasagiline, safinamide for MAO-B, Figure **1**) are shown in Tables **1** and **2**.

Structure−activity relationship studies. Following the previous results obtained for chromone-3-phenylcarboxamides (compounds **2-4**)[15], and in order to establish SAR f the MAO inhibitory activity of the newly developed chromone library (Figure **2**) was evaluated and the results are depicted in Tables **1** and **2**.

Table 1. MAO inhibitory activities of chromone-3- phenylcarboxamides **6-28** and standard inhibitors.

Compound	R	IC_{50} (nM)		SI
		*h*MAO-B	*h*MAO-A	
		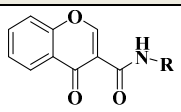		
2[15]		70.70 ± 1.70	*	>141 [b]
3[15]		2.90 ± 1.20	*	>3448 [b]
4[15]		8.00 ± 3.20	*	>1250 [b]
5[15]		1382 ± 25	*	>7.2 [b]
6		1.15 ± 0.16	*	>8696 [b]
7		11.43 ± 1.19	*	>875 [b]
8		7.30 ± 1.08	*	>1370 [b]
9		***	***	-
10		4574 ± 410	*	>2.2 [b]
11		7396 ± 84	*	>1.3 [b]
12	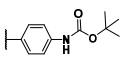	*	*	-
13		24.00 ± 1.10	*	>417 [b]

14		26.45 ± 2.11	*	>378 [b]
15		3.31 ± 0.25	*	>3021 [b]
16		427 ± 30	*	>23 [b]
17		1.03 ± 0.15	*	>9709 [b]
18		736 ± 12	*	>13 [b]
19		239 ± 21	*	>42
20		0.40 ± 0.023	**	>250000 [c]
21		1.33 ± 0.010	*	>7519 [b]
22		1.73 ± 1.01	*	>5780 [b]
23		2.65 ± 0.31	*	>3773 [b]
24		***	***	-
25		***	***	-
26		579 ± 30	*	>17 [b]
27		0.67 ± 0.13	**	>149254 [c]
28		31.61 ± 1.32	*	>316 [b]
R-(-)-Deprenyl	-	16.73 ± 1.48	68730 ± 421 [a]	4108
Rasagiline	-	49.66 ± 2.26	52974 ± 742	1067
Safinamide	-	23.07 ± 2.07	**	4335 [c]
Clorgyline	-	63410 ± 120	4.46 ± 0.32	0.000070

* Inactive at 10 μM; ** Inactive at 100 μM (highest concentration tested); *** Not soluble in DMSO;

[b] Values obtained under the assumption that the corresponding IC_{50} against MAO-A or MAO-B is the highest concentration tested (10 μM).

[c] Values obtained under the assumption that the corresponding IC_{50} against MAO-A or MAO-B is the highest concentration tested (100 μM).

SI: *h*MAO-B selectivity index = $IC_{50\ (hMAO\text{-}A)}$ /$IC_{50\ (hMAO\text{-}B)}$.

Effect of ring C substituents on MAO inhibitory activity. The introduction of halogens at the *para* position of the exocyclic ring yielded different results: iodine (compound **7**)

and fluorine (compound **8**) caused a decrease on activity when compared with the chlorine (compound **3**, IC_{50} = 2.90 nM), while bromine (compound **6**) led to a more potent compound (IC_{50} = 1.15 nM). Properties like atomic radius and/or electronegativity may thus play a significant role on the ligand-enzyme interaction. The evaluation of the effect of the introduction of a *p*-thiol substituent in compound **9** was not performed due to its poor solubility. The introduction of a *p*-amine substituent (compound **10**) was unfavorable, leading to a ~500-fold activity decrease when compared to the halogenated or methyl substituted derivatives (compounds **3, 4, 6-8**). This result is in accordance with recently published data, which showed that the introduction of a strong electron donating group (*p*-OH, compound **5**) decreased MAO-B inhibitory capacity (IC_{50} = 1382 nM).[15] Additionally, the presence of bulky *para* substituents led to a dramatic decrease (compound **11**) or complete loss (compound **12**) of MAO-B inhibitory activity. These observations also provided valuable data concerning the volume restrictions of the substituents on the exocyclic ring, since only small substituents seemed to favor an appropriate accommodation of the ligand on the enzyme's active site. The presence of the *p*-ethynyl (compound **13**, IC_{50} = 24.00 nM) and *p*-vinyl (compound **14**, IC_{50} = 26.45 nM) substituents yielded compounds with a remarkable inhibitory potency, although a superior activity was obtained for the saturated *p*-ethyl derivative (compound **15**, IC_{50} = 3.31 nM). The data showed that the presence of an unsaturated system in the mentioned position is not crucial for the IMAO-B activity of chromone-3-phenylcarboxamide based ligands. Overall, SAR studies indicated that the type of substituents on the exocyclic aromatic ring of chromone-3-phenylcarboxamide (Figure **1**) exerted a noteworthy influence on MAO-B inhibitory activity.

Subsequently, the effect of the most interesting substituents (Cl, Br, OH and CH_3) located at the *ortho* and *meta* positions of the exocyclic ring was evaluated. With the exception of the bromine group (compound **17**), the insertion of *o*-substituents (compounds **16** (Cl), **18** (OH) and **19** (CH_3)) resulted in a noticeably decrease on MAO-B inhibitory activity, when compared to the corresponding *para* derivatives (compounds **3-5**). However, when these substituents were located at the *meta* position (compounds **20** (Cl)**, 22** (OH) and **23** (CH_3)) a significant enhancement of IMAO-B potency was observed, with the exception of the *m*-bromine derivative (**21**), for which no potency change was observed. The type and position of substituents had a noteworthy effect on MAO-B inhibitory activity. In particular, the presence of a *m*-chlorine substituent at the aromatic exocyclic ring remarkably enhanced IMAO-B potency, with chromone **20** (IC_{50} = 0.40 nM and a SI >250000) emerging as the most potent and selective derivative.

Additional studies were performed with chromone carboxamides in which the exocyclic ring was derivatized with two or three chlorine or methyl substituents. However, the low solubility of the corresponding derivatives (compounds **24** and **25**) precluded their biological evaluation. Thus, the biological screening was only performed with the dimethyl (compounds **26** and **27**) and trimethyl (compound **28**) derivatives. Compound **27** (IC_{50} = 0.67 nM and a SI >149254) displayed a notorious increase of MAO-B potency and selectivity when compared with compound **4** (IC_{50} = 8.00 nM and a SI >1250), due to the introduction of a *m*-methyl substituent. However, when the same substituents were located at *ortho* and *meta* positions (compound **26**), a significant decrease of potency and selectivity (IC_{50} = 579 nM and a SI of 17) was observed. For compound **28,** with a third 5'-methyl group, a decrease on IMAO-B activity was also observed (IC_{50} = 31.61 nM).

SAR studies pointed that chromone-3-phenylcarboxamides with a *m*-chlorine substituent (**20**) or a 3',4'-dimethyl substituent (compound **27**) presented IMAO-B IC_{50} values within the picomolar range. Both compounds **20** (IC_{50} = 0.40 nM, SI >250000) and **27 (**IC_{50} = 0.67 *p*M, SI > 149254) showed respectively a 42- and 25-fold increase in inhibitory potency when compared to (*R*)-(−)-deprenyl, a 123- and 74-fold increase compared to rasagiline and, finally, a 57- and 34-fold increase compared to safinamide.

Effect of the spacer between the chromone and exocyclic aromatic ring. The insertion of a methyl group in the amide spacer completely abolished MAO inhibitory activity (compound **2** *vs* **29**). Similarly, the replacement of the amide nitrogen with oxygen (compound **4** *vs* **30**) caused a marked decrease of IMAO-B activity from 8.00 nM (compound **4**) to 2038 nM (compound **30**). A comparable outcome was observed when the nitrogen was replaced by sulphur (compound **4** *vs* **31**), with 67-fold decrease on IMAO-B activity observed for compound **31** (IC_{50} = 538 nM). This outcome suggests the inexorable significance of hydrogen bonding with the residues in the enzyme's active pocket. The importance of the carbonyl moiety was then subsequently explored. First, an exchange on the carbonyl and nitrogen group position (compound **4** *vs* **34**) was performed and the IMAO activity evaluated: although the compound was still active, a 12-fold decrease on IMAO-B activity (IC_{50} = 102 nM) was observed. As the results obtained so far indicated the importance of the spatial position of the amide group for the observed IMAO activity, a subsequent structural modification was performed in which the carbonyl group was removed (compound **36**). Biological screening of **36** showed that the presence of the amine yielded an active IMAO-B, a 71-fold decrease on inhibitory potency was observed (IC_{50} = 568 nM), suggesting that the carbonyl moiety is also a very important structural requirement to establish the appropriate interactions

with the target residues. To further characterize the importance of the location of the carboxamide spacer, a vinylic spacer between the pyrone ring and the carboxamide function of the chromone-3-phenylcarboxamide was introduced (compound **38**), leading to complete loss of MAO inhibitory activity. The same effect was observed when *p*-chlorine (compound **39**) or *p*-methyl (compound **40**) substituents were placed in the exocyclic aromatic ring and with the introduction of a 3′,4′-dimethyl substituent (compound **41**). The existence of a vinylic spacer may lead to steric constrains in the MAO-B pocket and, consequently, an unfavorable effect on activity. Moreover, the data reinforces the hypothesis established in our previous work, in which the carboxamide function linked directly to the pyrone ring ensured a key role in the ligand-enzyme complex.[11] The vinylic spacer present in compounds **38-41** may displace the carboxamide function from the appropriate binding site, leading to complete loss of MAO inhibitory activity.

Table 2. MAO inhibitory activities of chromone derivatives (**29-31, 34, 36** and **38-41**).

Compound	R	*h*MAO-B (IC_{50} in nM)	*h*MAO-A (IC_{50} in nM)	SI
29	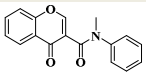	*	*	-
30	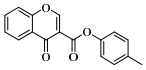	2038 ± 135	79455 ± 2974	39
31	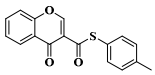	538 ± 46	1100 ± 78	2.0
34	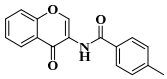	102 ± 9	*	>98 [b]
36	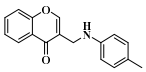	568 ± 38	94297 ± 7399	166.0
38	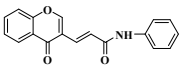	*	*	-
39	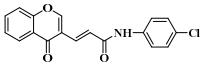	*	*	-
40	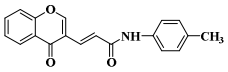	*	*	-
41	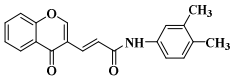	*	*	-

* Inactive at 10 μM (highest concentration tested);

[b] Values obtained under the assumption that the corresponding IC_{50} against MAO-A or MAO-B is the highest concentration tested (10 μM).

SI: *h*MAO-B selectivity index = $IC_{50\ (hMAO\text{-}A)}$ /$IC_{50\ (hMAO\text{-}B)}$.

Evaluation of drug-like properties. The 10 most potent and selective IMAO-B (compounds **3, 4, 6, 7, 15, 17, 20, 21, 22** and **27**) were selected and their drug-like properties calculated (Table **3**). The selection criteria was an IC_{50} towards human MAO-B < 12 nM and selectivity higher than 1000-fold for MAO-B over MAO-A. Remarkably, all the selected compounds were more potent *h*MAO-B inhibitors than the

standard inhibitors. The calculated physicochemical parameters include: molecular weight (MW), number of heavy atoms (N), partition coefficient (clog P), topological polar surface area (tPSA in Å^2), number of hydrogen acceptors (HBA), number of hydrogen donors (HBD) and number of rotatable bonds (*n*rotb) (Table **3**). In addition, the following multiparameter scores were also calculated: ligand-lipophilicity efficiency[21] (LLE), blood (plasma)-brain partitioning[22] (logBB) and absorption, distribution, metabolism, excretion and toxicity (ADMET) efficiency index[23] (AEI) (Table **3**). The same parameters were calculated for the MAO-B standard inhibitors selegiline, safinamide and rasagiline (Table **3**).

Overall, the selected chromones were in line with general drug-likeness requirements, namely concerning the well-known rule-of-5.[24] Additionally, they exhibited clogP and tPSA values within the optimal range for oral bioavailability and blood-brain barrier (BBB) permeability (log P 2−4, MW < 400 and tPSA 50−90 Å^2).[21,22,24,25] With the exception of compounds **7** and **15**, the multiparameter score LLE[21] obtained for all derivatives was within the optimal range for suitable drug candidates (5 < LLE < 7).[21] Chromones **20, 22** and **27** (LLE ≥ 6) may be suitable candidates for *in vivo* studies. Another key measurement is the prediction of BBB permeability properties, as determined by the logBB, which is the ratio of the steady-state concentrations of the drug in the brain and in the blood. Compounds with logBB below −1 are poorly distributed to the brain and are unlikely to function as effective CNS drugs.[22] All chromone derivatives depicted on Table **3** displayed logBB > −1, pointing towards potential BBB permeability. Incorporating the contribution of drug-transporters, the AEI score links lipophilic efficiency and ADMET properties. It has been suggested that AEI values over 7 identify compounds with improved ADMET properties.[23] In line with

the AEI score calculated for the new chiral IMAO-B safinamide, all the selected chromones displayed AEI > 7.[23]

Overall, the selected chromones presented drug-like properties similar to those of the standard inhibitor safinamide. Moreover, rasagiline and (R)-(−)-deprenyl have outlier behaviour for a significant number of parameters, including *N*, tPSA, log BB and AEI (see Table **3**).

Table 3. Drug-like properties of selected chromones and MAO-B standard inhibitors

Compound	MW[a]	pIC_{50}	*N*[a]	cLogP[a]	tPSA (Å^2)[a]	HBA[a]	HBD[a]	*n*rotb[a]	LLE	Log BB	AEI
3	299.71	8.54	21	3.31	59.31	4	1	2	5.23	-0.236	8.81
4	279.30	8.10	21	3.08	59.31	4	1	2	5.02	-0.271	8.46
6	344.16	8.94	21	3.45	59.31	4	1	2	5.49	-0.214	9.25
7	391.16	7.94	21	3.72	59.31	4	1	2	4.22	-0.173	7.12
15	293.32	8.48	22	3.55	59.31	4	1	3	4.93	-0.199	8.31
17	344.16	8.99	21	3.40	59.31	4	1	2	5.59	-0.222	9.42
20	299.71	9.39	21	3.29	59.31	4	1	2	6.10	-0.239	10.29
21	344.16	8.88	21	3.42	59.31	4	1	2	5.46	-0.219	9.20
22	281.27	8.76	21	2.13	79.54	5	2	2	6.63	-0.714	8.34
27	293.32	9.17	22	3.46	59.31	4	1	2	5.71	-0.213	9.64
Rasagiline	171.24	7.30	13	2.10	12.03	1	1	2	5.20	0.280	43.26
Safinamide	302.35	7.64	22	2.91	64.36	4	3	7	4.73	-0.371	7.34
(R)-(−)-Deprenyl	187.29	7.77	14	2.64	3.24	1	0	4	5.13	0.492	158.32
CNS^+ drugs[21-23, 26]	<450	___	___	<5	<60-70	<7	<3	<8	>5	≥ -1	___

MW: molecular weight; *N*: number of heavy atoms; clog P: calculated logarithm of the octanol-water partition coefficient; HBA: number of hydrogen acceptors; HBD: number of hydrogen donors; *n*rotb: number of rotatable bonds; LLE: ligand-lipophilicity efficiency; Log BB: logarithm of the ratio of the concentration of a drug in the brain and in the blood; AEI: ADMET efficiency index. [a] Properties calculated using Cheminformatics software [http://www.molinspiration.com].

Evaluation of enzyme-inhibition mechanism. To examine the inhibition mechanism of the most promising *h*MAO-B inhibitors (compounds **20** and **27**), kinetic experiments were performed. For this purpose, the initial rates of the MAO-B-catalyzed oxidation of *p*-tyramine at five different substrate concentrations, in the absence or presence of the selected chromone inhibitors at different concentrations, were measured. The results are depicted in Figure **4**. Graphical analyses of the reciprocal Lineweaver−Burk plots allowed the determination of Michaelis−Menten reaction kinetic parameters (Michaelis constant, K_m and maximum velocity, V_{max}). Concerning compound **20**, it was found that the V_{max} remained unchanged while K_m increased. The Lineweaver−Burk plots for different concentrations of **20** (Figure **4A**) were linear and intersected at the y-axis, indicating that this compound acted as a competitive IMAO-B. As for compound **27**, the K_m remained almost constant at different concentrations of the inhibitor whereas V_{max} decreased. The Lineweaver-Burk plots obtained for different concentrations of compound **27** (Figure **4B**) displayed a series of converging lines on the same point of the x-axis (1/[S]), profiling a non-competitive inhibition mechanism.

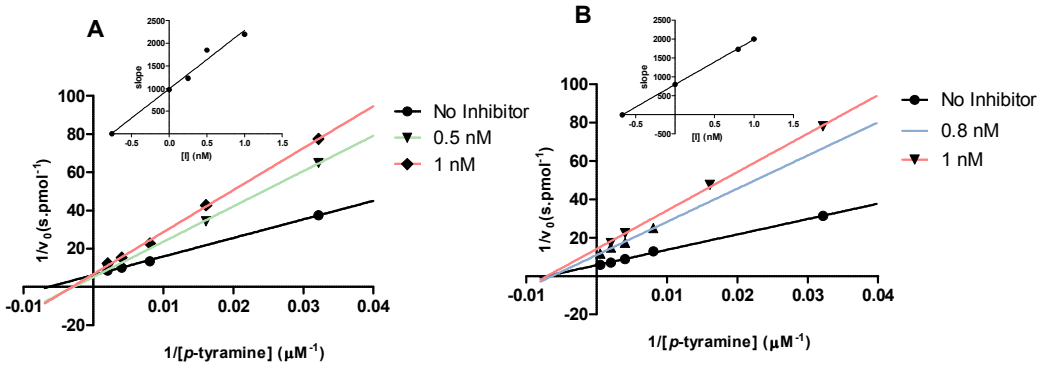

Figure 4 - Kinetic studies on the mechanism of *h*MAO-B inhibition by chromones **20** (Figure **4A**) and **27** (Figure **4B**). The effect of the inhibitors on the enzyme was determined from the double reciprocal plot of 1/rate (1/V) versus 1/substrate concentration in presence of varying concentrations of the inhibitors. The

Ki values were calculated by the intersection of the curves obtained by plotting 1/V versus the inhibitor concentration for each substrate concentration (Dixon plots insets on the top left).

From the Dixon plots, obtained from the replots of the slopes of the Lineweaver–Burk plots *vs* inhibitor concentrations (upper left corner), the *h*MAO-B inhibition binding affinities, determined as inhibition constants (*Ki*), were calculated. Chromones **20** (Figure **4A**) and **27** (Figure **4B**) displayed *Ki* values of 0.79 and 0.67 nM, respectively. The estimated *Ki* values correlated well with the inhibition mechanism suggested by the kinetic experiments: compound **20** (IC_{50} = 0.40 nM) displayed IC_{50} and *Ki* values slightly different but within the picomolar range, and compound **27** (IC_{50} = 0.67 nM), as is a non-competitive inhibitor, showed a *Ki* equal to its IC_{50}. Compound 27 can bind to the allosteric site distorting the 3D tertiary structure of the enzyme.

The reversibility of MAO-B inhibition by chromones **20** and **27** was then assessed by time-dependent inhibition studies. The behavior of standard irreversible ((*R*)-(−)-deprenyl and rasagiline) and reversible (safinamide) inhibitors was also evaluated under the same experimental conditions. *h*MAO-B activity (% of control) was measured along a 60 min incubation with the enzyme inhibitors (Figure **5**).

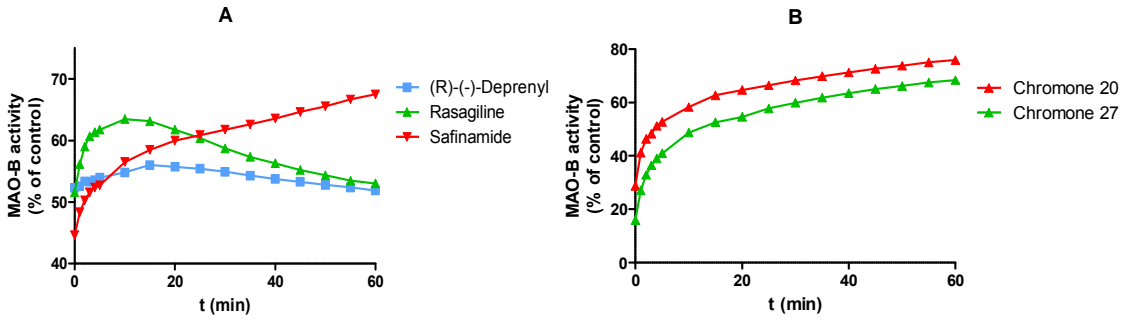

Figure 5. Time-dependent inhibition of recombinant human MAO-B by standard compounds (R)-(−)-deprenyl (50 nM), safinamide (40 nM) and rasagiline (200 nM) (Figure **4A**) and test compounds **20** (0.7

nM), and compound **27** (2 nM) (Figure **4B**). The remaining activity was expressed as % of activity. Data are the mean ± S.D. of three different experiments.

The analysis of time-dependent enzyme inhibition studies performed with the irreversible inhibitors (Figure **5A**) showed that the enzyme residual activity decayed continuously after the first 15 minutes of incubation, which is consistent with irreversible enzymatic inhibition. In case of the reversible inhibitor safinamide (Figure **5A**) an enhancement on enzymatic activity was observed along the analysis time. The same behavior was observed for chromones **20** and **27** (Figure **5B**), which points towards reversible MAO-B inhibition.

Modeling studies. The *h*MAOs binding modes of the most potent inhibitors, molecular modeling studies were carried out. Docking experiments were performed for compounds **20** and **27** with respect to *h*MAO-A and *h*MAO-B theoretical receptor models (see Experimental section). Both targets were recognized by the chromone based inhibitors by means of two opposite binding modes: a) with the chromone scaffold directed to the flavin adenine dinucleotide (FAD) cofactor (BMA) or b) towards the entrance gorge (BMB). Excluding **27** into the *h*MAO-A, whose BMB was predicted as best pose all best ranked complexes reported a BMA ligand accommodation. The graphical inspection of all sampled poses revealed BMA and BMB of **20** and **27** in both *h*MAOs (Table S1, Experimental section). All available docking score functions were in agreement to the experimentally observed *h*MAO-B selectivity. However, no correlation was observed comparing compounds' **20** and **27** different affinities. Actually, even if docking simulation suggested for both compounds a similar affinity with respect to the same target, **27** was predicted as more active than **20**. With the aim to progress in our analysis, ligand free targets (LF), the best poses

(TC) of **20** and **27** in both targets and the top ranked configuration opposite (SC) to the corresponding TC were submitted to explicit water solvent molecular dynamics simulation (Table **S1**, Figure S1, Experimental section). Firstly, the number of solvent water molecules available into the LF active sites and displaced by ligands TC and SC recognition was evaluated taking into account the molecular dynamics (MD) starting structures (Table **4**).

Table 4. Number of *h*MAOs active sites water molecules displaced by compounds **20** and **27** recognition in MD starting structures.

Target	Compound	Recognition	Displaced Waters
*h*MAO-A	**20**	TC	12
		SC	16
	27	TC	13
		SC	14
*h*MAO-B	**20**	TC	9
		SC	8
	27	TC	9
		SC	8

Such a preliminary analysis, and according to experimental selectivity data, addressed a desolvation penalty to *h*MAO-A recognition. Actually, both inhibitor binding modes always required the displacement of a larger number of water molecules in *h*MAO-A with respect to *h*MAO-B. Then, the perturbations of *h*MAOs conformational properties were investigated by comparing MD generated trajectories of the targets-inhibitors complexes with respect to the corresponding target ligand free (see Experimental section). The resulting RMSd matrix (Figure **S2**, Supplementary information) attained for both inhibitors clearly showed wider *h*MAO-A than *h*MAO-B distortions. Taking

into account that previous observation not appeared strictly dependent from the binding mode, an involvement of ligand steric hindrance in the isoform selectivity could be suggested. In fact, *h*MAO-A and *h*MAO-B active sites show similar primary structure but the former exhibits a monopartite substrate cavity whereas the second one has a larger and bipartite binding cleft. The differences in terms of shape and volume could reduce the *h*MAO-B perturbation induced by our ligands recognition. With the aim to understand the role of the chromone inhibitors exocyclic aromatic nucleous substituents and their contribution to the target binding, a graphical inspection of MD trajectories was performed (Figure **6**). This approach disclosed the favorable effect of the solvent in target recognition. In all trajectories, compounds **20** and **27** established stable water bridged hydrogen bonds to the *h*MAOs. In the case of compound **20** the water bridges involved also chlorine atom located on the exocyclic aromatic substituent. Such an atom also revealed target direct halogen bonds. Moreover, the MD frames graphical inspection highlighted a key role of stacking in complexes stabilization. In *h*MAO-A, Tyr407 established a π-π interaction with both TC and SC ligand orientation. The same contribution was also observed for *h*MAO-A Phe208 and, with lower frequency, for Tyr444. In *h*MAO-B, solvent molecules improved the ligands recognition, more remarkably than in *h*MAO-A: water bridges between chromone moiety and Tyr435 or Phe102 or between amide sp2 oxygen and Thr201 were observed in **20** TC and **27** SC, respectively. Notably, the compound **20** SC binding mode in *h*MAO-B showed a wide interaction network involving isoform exclusive residues: the ligand established hydrogen bond to Cys172 and stacking contacts to Tyr326 and Phe208 that in *h*MAO-A are replaced by Asn181, Ile335 and Ile199 respectively. Moreover during the MD simulation a water bridge was underlined between compound **20** chlorine atom and Tyr188 side chain.

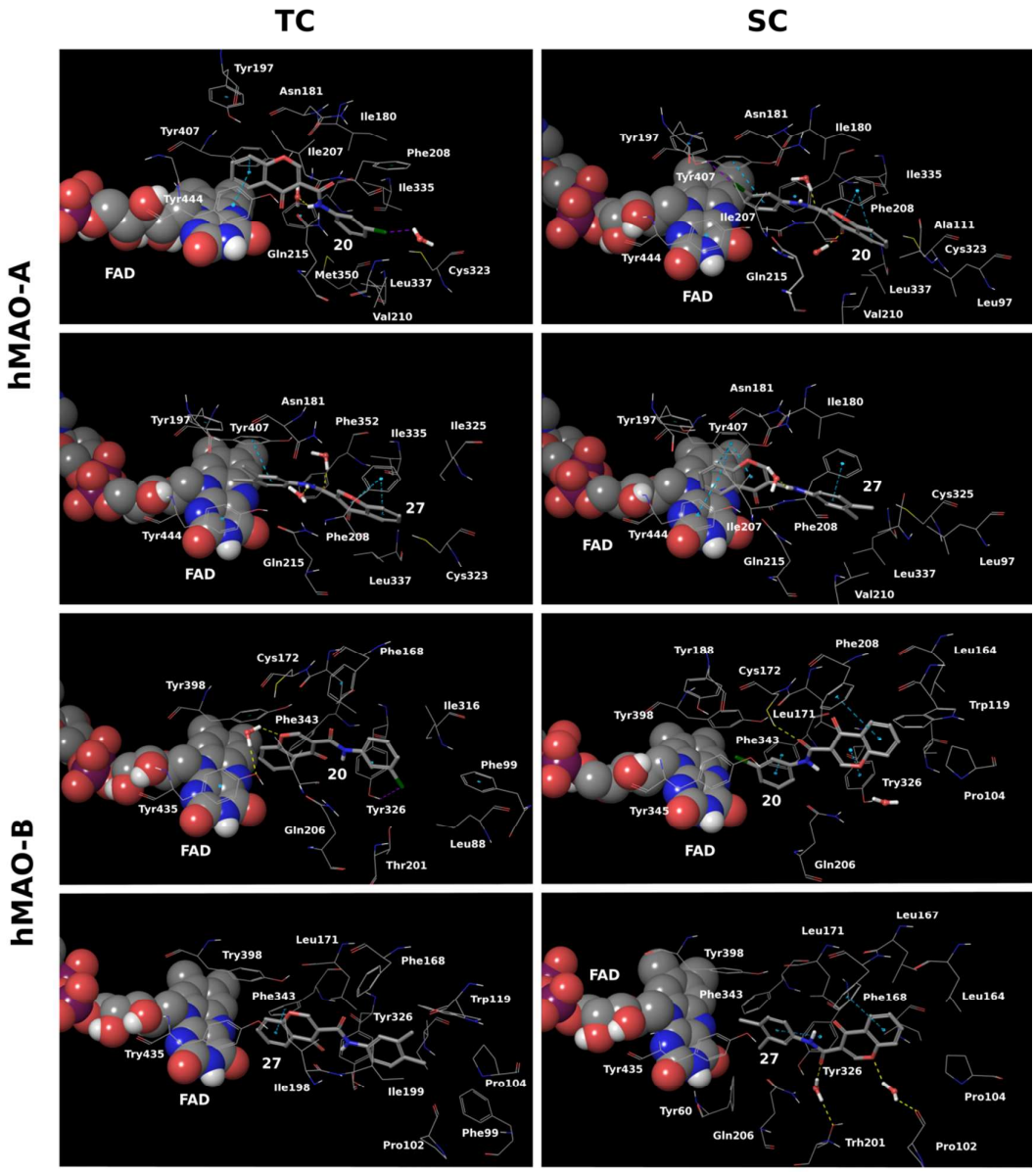

Figure 6. Last MD trajectory frames of **20** and **27** interacting to hMAO-A and hMAO-B. Ligands are depicted in polytube, FAD cofactor in spacefill, ligand interacting residues in wireframe and water molecules in ball and sticks notation. Chemical structures are CPK colour compliant. Cyan, purple or yellow dotted lines represent stacking contacts, halogen or hydrogen bonds respectively.

Compound **27** reported similar interactions with respect to **20**: stacking contacts were observed with *h*MAO-B Tyr326 and Ile199. Probably due to its steric hindrance, larger

than **20**, and due to the lack of the halogen atom, its *h*MAO-B recognition was less stable and its location within the active site was less deep preventing the hydrogen bond to Cys172.

Overall, the acquired data pointed out that chromone-3-phenylcarboxamides should not be considered as pan-assay interference compounds.[27] In fact, they are not MAO promiscuous ligands, as they behaved as selective MAO-B inhibitors with absent or negligible MAO-A activity. Furthermore, as shown for the most promising chromones, they did not behave as covalent inhibitors, since MAO-B inhibition was a reversible process. Furthermore, a good correlation between biological data and molecular docking experiences was attained.

Evaluation of the cytotoxicity. The cytotoxicity of the most promising compounds **20** and **27** was evaluated by the determination of the cellular viability in human neuroblastoma cells (SH-SY5Y cell line), after 24h incubation period and at two different concentrations (1 μM and 10 μM). Cellular viability was estimated using the methylthiazolyldiphenyl-tetrazolium bromide (MTT) reduction and the neutral red (NR) uptake assays. Metabolically active cells reduce MTT to formazan, which can be spectrophotometrically quantified, providing a direct measure of mitochondrial function.[28] The NR uptake assay is based on the ability of viable cells to incorporate and bind the supravital dye neutral red in the lysosomes, thus providing a quantitative estimation of the number of viable cells in culture. Control experiments were performed for both viability endpoints by adding vehicle (serum free medium with 0.1% DMSO) instead of the compound solution. The results obtained are shown in Figure **7**. In the MTT reduction assay, compound **20** caused a significant decrease on cellular viability, when compared to control groups (101.6 ± 11.7 %), for both concentrations (43.70 ±

5.98 % at 10 μM and 64.31 ± 5.96 % at 1 μM, $p < 0.001$) (Figure **7A**). For compound **27** no significant decrease on cellular viability was detected at 1 μM and only a slight decrease on the cellular viability was observed at 10 μM (74.55 ± 7.08 %, $p < 0.01$) (Figure **7A**). However, no significant decrease of the cellular viability for both compounds´ concentrations was observed when considering the NR uptake endpoint (Figure **7B**).

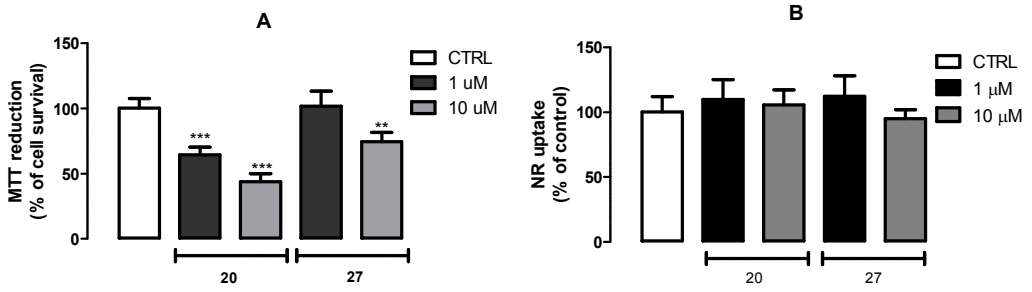

Figure 7. Cell viability of human neuroblastoma SH-SY5Y cells after a 24h exposure to chromones **20** and **27** at 1 and 10 μM as determined in the MTT reduction (**A**) and the NR uptake (**B**) assays. Untreated cells were used as control. ** $p < 0.01$ and *** $p < 0.001$.

Since the main effects were observed in the MTT reduction assay, the preliminary toxicological screening under the current experimental conditions points towards potential effects of **20** on mitochondrial function even at low concentrations (1 μM), which may be indicative of a potential drug-induced toxicity. Compound **27** showed only a mild mitochondrial effect at the highest concentration, suggesting a wider safety window.

Overall, the pharmacological and toxicological data acquired so far sustain the project progression wherein additional preclinical studies will be performed.

CONCLUSIONS

We successfully reported the optimization of the *N*-phenylchromone-3-carboxamide scaffold for the development of selective and reversible MAO-B inhibitors with subnanomolar potency. Structural optimization and SAR studies strengthen the importance of the amide spacer and the direct linkage of the carbonyl group to the γ-pyrone ring. While *o*-subsituents in the exocyclic ring generally led to a decrease on inhibitory potency, the presence of substituents in *meta* and *para* positions significantly enhanced MAO-B inhibition. The most potent and selective derivatives were *N*-(3'-chlorophenyl)-4-oxo-4H-chromene-3-carboxamide (**20**) (MAO-B IC_{50} = 0.40 nM), a competitive IMAO-B and *N*-(3',4'-dimethylphenyl)-4-oxo-4H-chromene-3-carboxamide (**27**) (MAO-B IC_50 = 0.67 nM), a non-competitive IMAO-B. Both acted as reversible MAO-B inhibitors with remarkable potency within the subnanomolar range and showed a drug-like profile similar to that of standard inhibitor safinamide. Computational docking studies provided insights into the inhibitors' interaction with the enzyme binding site and a rationale for their high potency. Compound **27** can be highlighted due to its wide safety range, as determined by preliminary cytotoxicity screenings in human neuroblastoma SH-SY5Y cells. Due to its appropriate physicochemical profile, which points towards BBB permeability, compound **27** is a valid candidate for subsequent animal studies and for the development of promising drug candidates for the therapy of neurodegenerative diseases.

EXPERIMENTAL SECTION

Chemistry. Reagents and general conditions. Chromone-3-carboxylic acid, 3-formylchromone, benzotriazol-1-yloxy)tripyrrolidinophosphonium hexafluorophosphate (PyBOP), pyridine, malonic acid, potassium carbonate, sodium sulphate, *N*,*N*-diisopropylethylamine (DIPEA), dimethylformamide (DMF), 1,8-diazabicycloundec-7-

ene (DBU), phosphorus oxychloride ($POCl_3$), aniline and its derivatives were purchased from Sigma-Aldrich Química S.A. (Sintra, Portugal). All other reagents and solvents were *pro analysis* grade and were acquired from Carlo Erba Reagents and Scharlab. and were used without additional purification.

Thin-layer chromatography (TLC) was carried out on precoated silica gel 60 F254 (Merck) with layer thickness of 0.2 mm. For analytical control the following systems were used: ethyl acetate/petroleum ether, ethyl acetate/methanol, chloroform/methanol, diethyl acetate in several proportions. The spots were visualized under UV detection (254 and 366 nm) and iodine vapor. Flash chromatography was performed using silica gel 60 0.2-0.5 or 0.040-0.063 mm (Carlo Erba Reagents). Following the workup, the organic phases were dried over Na_2SO_4. Solutions were decolorized with activated charcoal, when necessary. The recrystallization solvents were ethyl acetate, dichloromethane or ethyl ether/n-hexane. Solvents were evaporated in a Buchi Rotavapor.

The purity of the final products (>97% purity) was verified by high-performance liquid chromatography (HPLC) equipped with a UV detector. Chromatograms were obtained in an HPLC/DAD system, a Jasco instrument (pumps model 880-PU and solvent mixing model 880-30, Tokyo, Japan), equipped with a commercially prepacked Nucleosil RP-18 analytical column (250 mm x 4.6 mm, 5 μm, Macherey-Nagel, Duren, Germany), and UV detection (Jasco model 875-UV) at the maximum wavelength of 254 nm. The mobile phase consisted of a methanol/water or acetonitrile/water (gradient mode, room temperature) at a flow rate of 1 mL/min. The chromatographic data was processed in a Compaq computer, fitted with CSW 1.7 software (DataApex, Czech Republic).

Apparatus. NMR data were acquired, at room temperature, on a Brüker AMX 400 spectrometer operating at 400.15 MHz for ^{1}H and 100.62 MHz for ^{13}C. Chemical shifts were expressed in δ (ppm) values relative to tetramethylsilane (TMS) as internal reference; coupling constants (*J*) were given in Hz. Assignments were also made from DEPT (Distortionless Enhancement by Polarization Transfer) (underlined values). Electron impact mass spectra (EI-MS) were carried out on a VG AutoSpec instrument; the data were reported as *m/z* (% of relative intensity of the most important fragments). Microwave-assisted synthesis was performed in a Biotage Initiator Microwave Synthesizer. Melting point data were obtained in Stuart Scientic Melting Point SMP1.

A) Synthesis of chromone carboxamides (2-9, 11-29), ester (30) and thioester (31).

To a solution of chromone-3-carboxylic acid (**1**, 2.6 mmol) in DMF (4 mL) $POCl_3$ (2.6 mmol) was added. The mixture was stirred at room temperature for 30 min for the *in situ* formation of the acyl chloride. Then, an aromatic amine with the desired aromatic pattern (for compounds **2**-**9**, **11**-**29**), 4-methylphenol (for compound **30**), 4-methylbenzenethiol (for compound **31**) were added to the reaction. After 1-5 hours, the mixture was diluted with dichloromethane (20 mL), washed with H_2O (2 x 10 mL) and with saturated $NaHCO_3$ solution (2 x 10 mL). The organic phase was dried, filtered and concentrated under reduced pressure. The crude product was purified by flash chromatography and/or crystallization.

***N*-(4'-Bromophenyl)-4-oxo-4*H*-chromene-3-carboxamide (6).** The compound was obtained in 45% yield and recrystallized from DMF: mp 278−280 **°C.** ^{1}H NMR ($CDCl_3$) δ = 7.50 – 7.45 (2H, *m*, H3', H5'), 7.55 (1H, *ddd*, J = 8.1, 7.2, 1.0 Hz, H6), 7.61 (1H, *dd*, J = 8.5, 0.6 Hz, H8), 7.68 – 7.63 (2H, *m*, H2', H6'), 7.81 (1H, *ddd*, J = 8.7, 7.2, 1.7 Hz, H7), 8.34 (1H, *dd*, J = 8.0, 1.4 Hz, H5), 9.07 (1H, s, H2), 11.47 (1H, *s*, NH). ^{13}C

NMR ($CDCl_3$): 115.8 (C3), 117.1 (C4'), 118.6 (C8), 122.1 (C2', C6'), 124.0 (C4a), 126.3 (C6), 126.6 (C5), 132.0 (C3', C5'), 135.0 (C7), 137.1 (C1'), 156.2 (C8a), 160.8 (CONH), 162.9 (C2), 177.4 (C4). MS/EI *m/z* (%): 345 (M^++2, 31), 343 (M^+, 29), 173 (100), 121 (23).

***N*-(4'-Iodophenyl)-4-oxo-4*H*-chromene-3-carboxamide (7).** The compound was obtained in 16% yield and recrystallized from DMF: mp 277−280 **°C.** ^{1}H NMR ($CDCl_3$) δ = 7.60 – 7.53 (3H, *m*, H6, H3', H5'), 7.63 (1H, *d*, J = 8.5 Hz, H8), 7.72 – 7.66 (2H, *m*, H2', H6'), 7.83 (1H, *ddd*, J = 8.6, 7.2, 1.6 Hz, H7), 8.36 (1H, *dd*, J = 8.0, 1.5 Hz, H5), 9.09 (1H, *s*, H2), 11.48 (1H, *s*, NH). ^{13}C NMR ($CDCl_3$): δ = 87.9 (C4'), 116.0 (C3), 118.7 (C8), 122.5 (C2', C6'), 124.2 (C6), 126.4 (C5), 126.8 (C4a), 135.2 (C7), 137.2 (C1'), 138.1 (C3', C5'), 156.3 (C8a), 161.0 (CONH), 163.1 (C2), 177.6 (C4). MS/EI *m/z* (%): 390 (M^+, 93), 173 (100), 121 (25).

***N*-(4'-Fluorophenyl)-4-oxo-4*H*-chromene-3-carboxamide (8).** The compound was obtained in 23% yield and recrystallized from DMF: mp 254−257**°C.** ^{1}H NMR ($CDCl_3$) δ = 7.11 – 7.02 (2H, *m*, H3', H5'), 7.55 (1H, *ddd*, J = 8.1, 7.3, 1.0 Hz, H6), 7.61 (1H, *dd*, J = 8.5, 0.5 Hz, H8), 7.75 – 7.67 (2H, *m*, H2', H6'), 7.80 (1H, *ddd*, J = 8.7, 7.2, 1.7 Hz, H7), 8.34 (1H, *dd*, J = 8.0, 1.4 Hz, H5), 9.08 (1H, *s*, H2), 11.40 (1H, *s*, NH). ^{13}C NMR ($CDCl_3$): δ = 115.7 (*d*, J_{FC} = 22.5 Hz, C3', C5'), 115.9 (C3), 118.6 (C8), 122.2 (*d*, J_{FC} = 7.8.5 Hz, C2', C6'), 124.1 (C4a), 126.3 (C6), 126.6 (C5), 134.1 (*d*, J_{FC} = 2.8 Hz, C1'), 135.0 (C7), 156.2(C8a), 159.5 (*d*, J_{FC} = 244.7 Hz, C4'), 160.7 (CONH), 162.9 (C2), 177.5 (C4). MS/EI *m/z* (%): 384 (M^++1, 31), 383 (M^+, 94), 174 (43), 173 (100), 121 (81).

***N*-(4'-Mercaptophenyl)-4-oxo-4*H*-chromene-3-carboxamide (9).** The compound was obtained in 8% yield and recrystallized from AcOEt/*n*-hexane: mp >300 **°C.** ^{1}H NMR ($CDCl_3$) δ = 3.45 (1H, *s*, J = 8.8 Hz, SH), 7.30 (2H, *d*, J = 8.6 Hz, H3', H5'), 7.58 – 7.52 (1H, *m*, H6), 7.60 (1H, *d*, J = 8.4 Hz, H8), 7.64 (2H, *d*, J = 8.6 Hz, H2', H6'), 7.80 (1H, *ddd*, J = 8.6, 7.2, 1.6 Hz, H7), 8.33 (1H, *dd*, J = 8.0, 1.5 Hz, H5), 9.06 (1H, *s*, H2), 11.40 (1H, *s*, NH). ^{13}C NMR ($CDCl_3$): δ = 115.9 (C3), 118.6 (C8), 121.2 (C2', C6'), 124.1 (C4a), 125.5 (C4'), 126.3 (C6), 126.6 (C5), 130.7 (C7), 134.9 (C3', C5'), 136.3 (C1'), 156.2 (C8a), 160.7 (CONH), 162.9 (C2), 177.4 (C4). MS/EI *m/z* (%): 297 (M^+, 100), 173 (97), 121 (64).

***N*-(4'-(Dimethylamino)phenyl)-4-oxo-4*H*-chromene-3carboxamide (11).** The compound was obtained in 47% yield and recrystallized from CH_2Cl_2: mp 244−246 **°C.** ^{1}H NMR ($CDCl_3$) δ = 2.95 (6H, *s*, 2xCH_3), 6.76 (2H, *d*, J = 8.9 Hz, H3', H5'), 7.53 (1H, *ddd*, J = 8.1, 7.2, 1.1 Hz, Hz, H6), 7.64 – 7.57 (3H, m, H2', H6', H8), 7.78 (1H, *ddd*, J = 8.7, 7.1, 1.7 Hz, H7), 8.34 (1H, *dd*, J = 8.0, 1.7 Hz, H5), 9.07 (1H, s, H2), 11.17 (1H, *s*, NH). ^{13}C NMR ($CDCl_3$): δ = 41.0 (2xCH_3), 113.1 (C3', C5'), 116.3 (C3), 118.5 (C8), 121.9 (C2', C6'), 124.2 (C4a), 126.3 (C6), 126.4 (C5, C1'), 134.7, 156.2 (C8a, C4'), 160.1 (CONH), 162.5 (C2), 177.5 (C4). MS/EI *m/z* (%): 309 (M^++1, 26), 308 (M^+, 100), 135 (59), 120 (20).

***tert*-Butyl-(4-(4-oxo-4*H*-chromene-3-carboxamide)phenyl)carbamate (12).** The compound was obtained in 51% yield and recrystallized from AcOEt/*n*-hexane: mp 230−232 **°C.** ^{1}H NMR ($CDCl_3$) δ = 1.52 (9H, *s*, 3xCH_3), 6.47 (1H, *s*, OCONH), 7.41 – 7.33 (2H, *m*, H3', H5'), 7.54 (1H, *ddd*, J = 8.1, 7.2, 1.1 Hz, H6), 7.60 (1H, *dd*, J = 8.5, 0.6 Hz, H8), 7.70 – 7.65 (2H, *m*, H2', H6'), 7.79 (1H, *ddd*, J = 8.7, 7.2, 1.7 Hz, H7),

8.34 (1H, *dd*, J = 8.0, 1.4 Hz, H5), 9.07 (1H, *s*, H2), 11.34 (1H, *s*, CONH). ^{13}C NMR($CDCl_3$) δ = 28.4 ($C(\underline{C}H_3)_3$), 80.5 ($\underline{C}(CH_3)_3$), 116.1 (C3), 118.5 (C8), 119.1 (C3',C5'), 121.2 (C2',C6'), 124.1 (C4a), 126.3 (C6), 126.5 (C5), 133.4 (C1', C4'), 134.9 (C7), 152.8 (OCONH), 156.2 (C8a), 160.5 (CONH), 162.7 (C2), 177.5 (C4). MS/EI *m/z* (%): 380 (M^+, 45), 325 (87), 324 (98), 306 (60), 280 (100), 173 (98), 121 (98).

***N*-(4'-Ethynylphenyl)-4-oxo-4*H*-chromene-3-carboxamide (13).** The compound was obtained in 28% yield and recrystallized from CH_2Cl_2: mp 240−242 **°C.** ^{1}H NMR ($CDCl_3$) δ = 3.06 (1H, *s*, CCH), 7.52 – 7.46 (2H, *m*, H3', H5'), 7.55 (1H, *ddd*, J = 8.1, 7.2, 1.0 Hz, H6), 7.60 (1H, *dd*, J = 8.5, 0.6 Hz, H8), 7.75 – 7.69 (2H, *m*, H2', H6'), 7.80 (1H, *ddd*, J = 8.7, 7.2, 1.7 Hz, H7), 8.34 (1H, *dd*, J = 8.0, 1.6 Hz, H5), 9.07 (1H, *s*, H2), 11.52 (1H, *s*, NH). ^{13}C NMR ($CDCl_3$): δ = 76.8 (C$\underline{C}$H), 83.5 ($\underline{C}$CH), 115.9 (C3), 117.8 (C4'), 118.6 (C8), 120.2 (C2',C6'), 124.1 (C4a), 126.3 (C6), 126.6 (C5), 133.0 (C3',C5'), 135.0 (C7), 138.5 (C1'), 156.2 (C8a), 160.8 (CONH), 163.0 (C2), 177.4 (C4). EI/ME *m/z* (%): 290 (M^++1, 62), 289 (M^+, 95), 174 (55), 173 (100), 121 (83).

***N*-(4'-Vinylphenyl)-4-oxo-4*H*-chromene-3-carboxamide (14).** The compound was obtained in 33% yield and recrystallized from CH_2Cl_2: mp 238−241 **°C.** ^{1}H NMR ($CDCl_3$) δ = 5.21 (1H, *dd*, J = 10.9, 0.8 Hz, CHC$\underline{H}_2$), 5.71 (1H, *dd*, J = 17.6, 0.9 Hz, CHC$\underline{H}_2$), 6.70 (1H, *dd*, J = 17.6, 10.9 Hz, C$\underline{H}$CH$_2$), 7.46 – 7.38 (2H, *m*, H2', H6'), 7.55 (1H, *ddd*, J = 8.1, 7.2, 1.1 Hz, H6), 7.60 (1H, *dd*, J = 8.5, 0.6 Hz, H8), 7.75 – 7.69 (2H, *m*, H3', H5'), 7.80 (1H, *ddd*, J = 8.7, 7.1, 1.7 Hz, H7), 8.34 (1H, *dd*, *J* = 8.0, 1.7 Hz, H5), 9.08 (1H, *s*, H2), 11.44 (1H, *s*, NH). ^{13}C NMR ($CDCl_3$): δ = 113.2 (CH$\underline{C}$H$_2$), 116.1 (C3), 118.7 (C8), 120.6 (C2',C6'), 124.2 (C4a), 126.4 (C6), 126.7 (C5), 127.0

(C3',C5'), 134.8 (C4'), 135.1 (C7), 136.4 ($\underline{C}HCH_2$), 137.7 (C1'), 156.3 (C8a) , 160.8 (CONH), 163.0 (C2), 177.6 (C4). MS/EI *m/z* (%): 291 (M^+, 78), 173 (100), 121 (30).

***N*-(4'-Ethylphenyl)-4-oxo-4*H*-chromene-3-carboxamide (15).** The compound was obtained in 45% yield and recrystallized from CH_2Cl_2: mp 199−202 **°C.** ^{1}H NMR ($CDCl_3$) δ = 1.24 (3H, *t*, J = 7.6 Hz,$CH_2C\underline{H_3}$), 2.64 (2H, *q*, J = 7.6 Hz, $C\underline{H_2}CH_3$), 7.24 – 7.16 (2H, *m*, H3', H5'), 7.54 (1H, *ddd*, J = 8.1, 7.2, 1.1 Hz, H6), 7.60 (1H, *dd*, J = 8.5, 0.6 Hz, H8), 7.68 – 7.62 (2H, *m*, H2', H6'), 7.79 (1H, *ddd*, J = 8.7, 7.2, 1.7 Hz, H7), 8.34 (1H, *dd*, J = 8.0, 1.7 Hz, H8), 9.08 (1H, *s*, H2), 11.33 (1H, *s*, NH). ^{13}C NMR ($CDCl_3$): δ = 15.8 ($CH_2\underline{C}H_3$), 28.5 ($\underline{C}H_2CH_3$), 116.3 (C3), 118.7 (C8), 120.8 (C2',C6'), 124.3 (C4a), 126.4 (C6), 126.6 (C5), 128.5 (C3',C5'), 135.0 (C7), 135.8 (C1'), 140.7 (C4'), 156.4 (C8a), 160.7 (CONH), 162.9 (C2), 177.6 (C4). MS/EI *m/z* (%): 293 (M^+, 74), 278 (37), 173 (100), 121 (31).

***N*-(2'-Chlorophenyl)-4-oxo-4*H*-chromene-3-carboxamide (16).** The compound was obtained in 53% yield and recrystallized from CH_2Cl_2: mp 240−242 **°C.** ^{1}H NMR ($CDCl_3$) δ = 7.08 (1H, *ddd*, J = 8.0, 7.5, 1.6 Hz, H4'), 7.30 (1H, *ddd*, J = 8.7, 1.5, 0.7 Hz, H5'), 7.44 (1H, *dd*, J = 8.0, 1.5 Hz, H3'), 7.53 (1H, *ddd*, J = 8.1, 7.2, 1.1 Hz, H6), 7.59 (1H, *dd*, J = 8.5, 0.6 Hz, H8), 7.78 (1H, *ddd*, J = 8.6, 7.2, 1.7 Hz, H7), 8.39 (1H, *dd*, J = 8.0, 1.7 Hz, H5), 8.56 (1H, *dd*, J = 8.3, 1.5 Hz, H5'), 9.08 (1H, *s*, H2), 11.81 (1H, *s*, NH). ^{13}C NMR ($CDCl_3$): δ = 116.2 (C3), 118.6 (C8), 122.6 (C6), 124.1 (C4a), 124.2 (C2'), 125.0 (C5'), 126.6 (C5), 126.7 (C6'), 127.6 (C3'), 129.5 (C4'), 135.0 (C7'), 135.5 (C1'), 156.3 (C8a), 161.2 (CONH), 163.2 (C2), 177.4 (C4). MS/EI *m/z* (%): 301 (M^++2, 24), 299 (M^+, 69), 265 (83), 264 (95), 265 (83), 174 (54), 173 (97), 121 (100).

***N*-(2'-Bromophenyl)-4-oxo-4*H*-chromene-3-carboxamide (17).** The compound was obtained in 36% yield and recrystallized from DMF: mp 186−189 °C. ^{1}H NMR ($CDCl_3$) δ = 7.02 (1H, *ddd*, J = 8.0, 7.4, 1.6 Hz, H4'), 7.39 – 7.29 (1H, *m*, H5'), 7.54 (1H, *ddd*, J = 8.1, 7.2, 1.0 Hz, H6), 7.65 – 7.58 (2H, *m*, H8, H6'), 7.79 (1H, *ddd*, J = 8.6, 7.2, 1.7 Hz, H7), 8.40 (1H, *dd*, J = 8.0, 1.6 Hz, H5), 8.51 (1H, *dd*, J = 8.3, 1.5 Hz, H3'), 9.08 (1H, *s*, H2), 11.70 (1H, *s*, NH). ^{13}C NMR ($CDCl_3$): δ = 114.4 (C3), 116.2 (C2'), 118.6 (C8), 123.2 (C6'), 124.3 (C2a), 125.6 (C6), 126.6 (C5), 126.7 (C5'), 128.2 (C4'), 132.8 (C3'), 135.0 (C7), 136.8 (C1'), 156.3 (C8a), 161.3 (CONH), 163.2 (C2), 177.3 (C4). MS/EI *m/z* (%): 345 (M^++2, 26), 343 (M^+, 27), 265 (58), 264 (100), 173 (69), 121 (38).

***N*-(2'-Hydroxyphenyl)-4-oxo-4*H*-chromene-3-carboxamide (18).** The compound was obtained in 31% yield and recrystallized from MeOH/CH_2Cl_2: mp 252−255 °C. ^{1}H NMR (DMSO-*d6*) δ = 6.90 – 6.74 (1H, *m*, H5'). 7.02 – 6.90 (2H, *m*, H3', H4'), 7.64 (1H, *dd*, J = 7.5, 7.5 Hz, H6), 7.82 (1H, d, J = 8.4 Hz, H8), 8.00 – 7.88 (1H, *m*, H7), 8.27 (1H, *dd*, J = 8.0, 1.6 Hz, H5), 8.44 – 8.31 (1H, *m*, H6'), 9.19 (1H, *s*, H2), 10.16 (1H, *s*, OH), 11.58 (1H, *s*, NH).^{13}C NMR (DMSO-*d6*): δ = 114.7 (C3'), 115.6 (C3), 118.8 (C8), 119.1 (C5'), 120.2 (C6), 123.6 (C4a), 124.1 (C4'), 125.7 (C6), 126.7 (C1'), 126.8 (C5), 135.4 (C7), 146.6 (C2'), 155.7 (C8a), 160.1 (CONH), 163.6 (C2), 176.6 (C4). MS/EI *m/z* (%): 281 (M^+, 100), 173 (100), 121 (42).

***N*-(*o*-Tolyl)-4-oxo-4*H*-chromene-3-carboxamide (19).** The compound was obtained in 61% yield and recrystallized from CH_2Cl_2: mp 179−182 °C. ^{1}H NMR ($CDCl_3$) δ = 2.48 (3H, *s*, CH_3), 7.08 (1H, *ddd*, J = 7.5, 7.5, 1.2 Hz, H4'), 7.28 – 7.21 (2H, *m*, H5', H6'), 7.54 (1H, *ddd*, J = 8.1, 7.2, 1.1 Hz, H6), 7.60 (1H, *dd*, J = 8.5, 0.6 Hz, H8), 7.79 (1H,

ddd, J = 8.7, 7.2, 1.7 Hz, H7), 8.27 (1H, *d*, J = 8.1 Hz, H3'), 8.36 (1H, *dd*, J = 8.0, 1.7 Hz, H5), 9.10 (1H, *s*, H2), 11.29 (1H, *s*, NH). ^{13}C NMR ($CDCl_3$): 18.4 (CH_3), 116.4 (C3), 118.7 (C8), 122.1 (C6'), 124.3 (C4a), 124.7 (C5'), 126.5 (C6), 126.6 (C5), 126.8 (C4'), 128.5 (C2'), 130.5 (C3'), 135.0 (C7), 136.6 (C1'), 156.3 (C8a), 160.9 (CONH), 163.1 (C2), 177.7 (C4). MS/EI *m/z* (%): 279 (M^+, 61) 260 (44), 173 (100), 121 (61).

***N*-(3'-Chlorophenyl)-4-oxo-4*H*-chromene-3-carboxamide (20).** The compound was obtained in 40% yield and recrystallized from CH_2Cl_2: mp 239−242 °C. ^{1}H NMR (DMSO-*d6*) δ = 7.21 (1H, *ddd*, J = 8.0, 2.1, 0.9 Hz, H4'), 7.42 (1H, *dd*, *J* = 8.1, 8.1 Hz, H5'), 7.57 (1H, *ddd*, J = 8.2, 2.0, 0.9 Hz, H6'), 7.66 (1H, *ddd*, J = 8.1, 7.1, 1.1 Hz, H6), 7.84 (1H, *dd*, J = 8.5, 0.6 Hz, H8), 7.96 (1H, *ddd*, *J* = 8.7, 7.1, 1.7 Hz, H7), 8.00 (1H, *dd*, J = 2.0, 2.0 Hz, H2'), 8.25 (1H, *dd*, J = 8.0, 1.3 Hz, H5), 9.20 (1H, *s*, H2), 11.40 (1H, *s*, NH). ^{13}C NMR (DMSO-*d6*): δ = 115.5 (C3), 118.5 (C8), 118.8 (C6'), 119.5 (C2'), 123.4 (C6), 123.9 (C4a), 125.6 (C5), 126.8 (C4'), 130.7 (C5'), 133.3 (C3'), 135.5 (C7), 139.4 (C1'), 156.7 (C8a), 160.8 (CONH), 163.6 (C2), 176.5 (C4). MS/EI *m/z* (%): 301 (M^++2, 42), 299 (M^+, 85), 174 (29), 173 (100), 121 (70).

***N*-(3'-Bromophenyl)-4-oxo-4*H*-chromene-3-carboxamide (21).** The compound was obtained in 42% yield and recrystallized from CH_2Cl_2: mp 249−252 °C. ^{1}H NMR ($CDCl_3$) δ = 7.40-7.32 (2H, *m*, H4', H5'), 7.63-7.59 (1H, *m*, H6'), 7.66 (1H, *ddd*, J = 8.1, 7.1, 1.1 Hz, H6), 7.84 (1H, dd, J = 8.5, 0.6 Hz, H8), 7.96 (1H, *ddd*, J = 8.6, 7.1, 1.7 Hz, H7), 8.14 (1H, *dd*, J = 2.4, 1.4 Hz, H2'), 8.25 (1H, *dd*, J = 8.0, 1.3 Hz, H5), 9.19 (1H, *s*, H2), 11.38 (1H, *s*, NH). MS/EI *m/z* (%): 345 (M^++2, 51), 343 (M^+, 51), 173 (100), 121 (43).

***N*-(3'-Hydroxyphenyl)-4-oxo-4*H*-chromene-3-carboxamide (22).** The compound was obtained in 42% yield and recrystallized from DMF: mp 284−287 °C. ^{1}H NMR (DMSO-*d6*) δ = 6.55 (1H, *ddd*, J = 8.1, 2.3, 0.7 Hz, H4'), 7.02 (1H, *d*, J = 8.2 Hz, H6'), 7.16 (1H, *dd*, J = 8.0, 8.0 Hz, H5'), 7.32 (1H, *dd*, J = 2.1, 2.1 Hz, H2'), 7.65 (1H, *dd*, J = 7.6 Hz, H6), 7.82 (1H *d*, J = 8.5 Hz, H8), 7.95 (1H, *dd*, J = 7.8, 7.8 Hz, H7), 8.25 (1H, *d*, J = 7.9 Hz, H5), 9.17 (1H, *s*, H2), 9.53 (1H, *s*, OH), 11.22 (1H, *s*, NH). ^{13}C NMR (DMSO-*d6*): δ = 106.9 (C2'), 110.5 (C6'), 111.3 (C4'), 115.7 (C3), 118.8 (C8), 123.4 (C4a), 125.6 (C6), 126.7 (C5), 129.8 (C5'), 135.5 (C7), 139.0 (C1'), 155.7 (C8a), 157.9 (C3'), 160.2 (CONH), 163.4 (C2), 176.8 (C4). MS/EI *m/z* (%): 281 (M^+, 100), 173 (98), 121 (47).

***N*-(*m*-Tolyl)- 4-oxo-4*H*-chromene-3-carboxamide (23).** The compound was obtained in 45% yield and recrystallized from MeOH/CH_2Cl_2: mp 214−215 °C. ^{1}H NMR ($CDCl_3$) δ = 2.38 (3H, *s*, CH_3), 6.98 – 6.94 (1H, m, H4'), 7.25 (1H, *dd*, J = 7.8 7.8 Hz, H5'), 7.62 – 7.52 (4H, m, H2', H6', H6, H8), 7.79 (1H, *ddd*, J = 8.7, 7.2, 1.7 Hz, H7), 8.34 (1H, *dd*, J = 8.0, 1.7 Hz, H5), 9.07 (1H, *s*, H2), 11.35 (1H, *s*, NH). ^{13}C NMR ($CDCl_3$): 21.5 (CH_3), 116.1 (C3), 117.7 (C6'), 118.5 (C8), 121.2 (C4'), 124.1 (C4a), 125.3 (C2'), 126.3 (C6), 126.5 (C5), 128.9 (C5'), 134.9 (C7), 137.9 (C3'), 138.9 (C1'), 156.2 (C8a), 160.7 (CONH), 162.8 (C2), 177.5 (C4). MS/EI *m/z* (%): 279 (M^+, 66), 173 (100), 121 (35).

***N*-(3',4'-Dichlorophenyl)-4-oxo-4*H*-chromene-3-carboxamide (24)**. The compound was obtained in 59% yield and recrystallized from DMF: mp >300 °C. ^{1}H NMR ($CDCl_3$) δ = 7.44 (1H, *d*, J = 8.7 Hz, H5'), 7.70 – 7.54 (3H, *m*, H6, H8, H6'), 7.84 (1H, *ddd*, J = 8.6, 7.2, 1.7 Hz, H7), 8.04 (1H, *d*, J = 2.4 Hz, H2'), 8.36 (1H, *dd*, J = 8.0, 1.4

Hz, H5), 9.09 (1H, *s*, H2), 11.57 (1H, *s*, NH). MS/EI *m/z* (%): 337 (M^++4, 30), 336 (M^++3, 30), 335 (M^++2, 88), 334 (M^++1, 45), 333 (M^+, 100), 174 (57), 173 (94), 121 (98).

***N*-(3',4',5'-Trichlorophenyl)-4-oxo-4*H*-chromene-3-carboxamide (25).** The compound was obtained in 88% yield and recrystallized from DMF: mp 300−303 °C. ^{1}H NMR ($CDCl_3$) δ = 7.57 (1H, *ddd*, J = 8.1, 7.2, 1.0 Hz, H6), 7.62 (1H, *dd*, J = 8.5, 0.5 Hz, H8), 7.83 (1H, *ddd*, J = 8.7, 7.2, 1.7 Hz, H7), 7.88 (2H, *s*, H2', H6'), 8.34 (1H, *dd*, J = 8.0, 1.4 Hz, H5), 9.06 (1H, *s*, H2), 11.61 (1H, *s*, NH). EI/ME *m/z* (%): 371 (M^++4, 14), 370 (M^++3, 7), 369 (M^++2, 43), 368 (M^++1, 8), 367 (M^+, 45), 174 (20), 173 (100), 121 (46).

***N*-(2',3'-Dimethylphenyl)-4-oxo-4*H*-chromene-3-carboxamide (26).** The compound was obtained in 26% yield and recrystallized from MeOH/CH_2Cl_2: mp 197−200 °C. ^{1}H NMR ($CDCl_3$) δ = 2.33 (3H, *s*, CH_3), 2.34 (3H, *s*, CH_3), 7.00 (1H, *d*, J = 7.5 Hz, H4'), 7.14 (1H, *dd*, J = 7.8, 7.8 Hz, H5'), 7.53 (1H, *ddd*, J = 8.1, 7.2, 1.1 Hz, H6), 7.59 (1H, *dd*, J = 8.5, 0.6 Hz, H8), 7.78 (1H, *ddd*, J = 8.7, 7.1, 1.7 Hz, H7), 7.97 (1H, *d*, J = 8.1 Hz, H6'), 8.35 (1H, *dd*, J = 8.0, 1.3 Hz, H5), 9.08 (1H, *s*, H2), 11.21 (1H, *s*, NH). ^{13}C NMR ($CDCl_3$): δ = 13.8 (CH_3), 20.7 (CH_3), 116.2 (C3), 118.4 (C8), 120.7 (C6'), 124.1 (C4a), 125.8 (C5'), 126.2 (C4'), 126.4 (C6), 126.6 (C5), 127.8 (C2'), 134.8 (C7), 136.0 (C1'), 137.1 (C3'), 156.1 (C8a), 160.8 (CONH), 162.8 (C2), 177.5 (C4). MS/EI *m/z* (%): 295 (M^++3, 39) 294 (M^++2, 50), 293 (M^+, 65), 174 (52), 173 (40), 121 (100).

***N*-(3',4'-Dimethylphenyl)-4-oxo-4*H*-chromene-3-carboxamide (27).** The compound was obtained in 23% yield and recrystallized from CH_2Cl_2: mp 233−236 °C. ^{1}H NMR

(CDCl$_3$) δ = 2.25 (3H, *s*, CH$_3$), 2.28 (3H, *s*, CH$_3$), 7.12 (1H, *d*, J = 8.1 Hz, H5'), 7.48 (1H, *dd*, J = 8.1, 2.2 Hz, H6'), 7.56 – 7.50 (2H, *m*, H2', H6), 7.59 (1H, *dd*, J = 8.5, 0.6 Hz, H8), 7.79 (1H, *ddd*, J = 8.7, 7.1, 1.7 Hz, H7), 8.34 (1H, *dd*, J = 8.0, 1.7 Hz, H5), 9.07 (1H, *s*, H2), 11.28 (1H, *s*, NH). ^{13}C NMR (CDCl$_3$): δ = 19.2 (CH$_3$), 19.9 (CH$_3$), 116.2 (C3), 118.0 (C8), 118.5 (C6'), 121.8 (C2'), 124.1 (C4a), 126.3 (C6), 126.5 (C5), 130.0 (C5'), 132.8 (C4'), 134.8 (C7), 135.7 (C3'), 137.2 (C1'), 156.2 (C8a), 160.5 (CONH), 162.7 (C2), 177.5 (C4). MS/EI *m/z* (%): 294 (M^++1, 34), 293 (M^+, 88,), 173 (100), 121 (62).

***N*-(3',4',5'-Trimethylphenyl)-4-oxo-4*H*-chromene-3-carboxamide (28).** The compound was obtained in 32% yield and recrystallized from MeOH: mp 251−253 **°C.** ^{1}H NMR (CDCl$_3$) δ = 2.15 (3H, *s*, J = 7.0 Hz, CH$_3$), 2.30 (6H, *s*, 2xCH$_3$), 7.40 (2H, *s*, H2', H6'), 7.53 (1H, *ddd*, J = 8.1, 7.2, 1.0 Hz, H6), 7.59 (1H, *dd*, J = 8.5, 0.6 Hz, H8), 7.78 (1H, *ddd*, J = 8.7, 7.1, 1.7 Hz, H7), 8.33 (1H, *dd*, J = 8.0, 1.4 Hz, H5), 9.06 (1H, *s*, H2), 11.22 (1H, *s*, NH). ^{13}C NMR (CDCl$_3$): δ = 15.0 (CH$_3$), 20.7 (2xCH$_3$), 116.2 (C3), 118.5 (C8), 119.7 (C2', C6'), 124.2 (C4a), 126.3 (C6), 126.4 (C5), 131.4 (C1'), 134.8 (C7), 135.0 (C5, 137.1 (C3', C5'), 156.2 (C8a), 160.4 (CONH), 162.7 (C2), 177.5 (C4). MS/EI *m/z* (%): 307 (M^+, 42,), 253 (100), 183 (51), 173 (55).

***N*-Methyl-*N*-phenyl-4-oxo-4*H*-chromene-3-carboxamide (29).** The compound was obtained in 75% yield and recrystallized from CH_2Cl_2: mp 182−185 **°C.** ^{1}H NMR (DMSO-*d6*) δ = 3.34 (3H, *s*, CH$_3$), 7.17 (1H, *bs*, H4'), 7.28 (4H, *bs*, H2', H3', H5', H6'), 7.45 (2H, *dd*, J = 6.2, 6.2 Hz, H6'), 7.58 (1H, *d*, J = 6.4 Hz, H8), 7.77 (1H, *dd*, J = 6.9, 6.9 Hz, H7), 7.92 (1H, *bs*, H8), 8.47 (1H, *s*, H2). ^{13}C NMR (CDCl$_3$): δ = 36.9 (CH$_3$), 118.5 (C8), 123.1 (C3), 123.4 (C4a), 125.1 (C6), 125.9 (C5), 126.9 (C2', C6'),

127.3 (C4'), 129.0 (C3', C5'), 134.6 (C7), 143.3 (C1'), 155.4 (C4a), 156.1 (C2), 163.1 (COON), 172.9 (C4). MS/EI *m/z* (%): 279 (M^+, 72), 185 (21), 173 (100), 121 (67), 106.0 (38).

***O*-(*p*-Tolyl)-4-oxo-4*H*-chromene-3-carboxylate (30).** The compound was obtained in 14% yield and recrystallized from CH_2Cl_2: mp 165−168 °C. ^{1}H NMR ($CDCl_3$) δ = 2.37 (3H, *s*, CH_3), 7.13 – 7.09 (2H, *m*, H3', H5'), 7.24 – 7.18 (2H, *m*, H2', H6'), 7.50 (1H, *ddd*, J = 8.1, 7.2, 1.1 Hz, H6), 7.54 (1H, *dd*, J = 8.5, 0.6 Hz, H8), 7.77 – 7.71 (1H, *m*, H7), 8.33 (1H, *dd*, J = 8.1, 1.5 Hz, H5), 8.85 (1H, *s*, H2).^{13}C NMR ($CDCl_3$): δ = 29.9 (CH_3), 115.8 (C3), 118.2 (C8), 121.4 (C2', C6'), 125.2 (C4a), 126.5 (C6), 126.7 (C5), 130.0 (C3', C5'), 134.4 (C7), 135.8 (C4'), 148.1 (C1'), 155.7 (C8a), 162.0 (COO), 162.6 (C2), 173.2 (C4). MS/EI *m/z* (%): 280 (M^+, 44), 173 (100), 121 (70).

***S*-(*p*-Tolyl)-4-oxo-4*H*-chromene-3-carbothioate (31).** The compound was obtained in 26% yield and recrystallized from CH_2Cl_2/*n*-hexane: mp 155−158 °C. ^{1}H NMR ($CDCl_3$) δ = 2.43 (3H, *s*, CH_3), 7.32 – 7.27 (2H, *m*, H2', H6), 7.45 – 7.40 (2H, *m*,' H3', H5'), 7.59 – 7.52 (2H, *m*, H6, H8), 7.78 (1H, *ddd*, J = 8.7, 7.2, 1.7 Hz, H7), 8.39 (1H, *dd*, J = 8.0, 1.5 Hz, H5), 8.71 (1H, *s*, H2). ^{13}C NMR ($CDCl_3$): δ = 21.5 (CH_3), 118.4 (C8), 121.4 (C3), 124.7 (C4a), 125.0 (C1'), 126.70 (C6), 126.72 (C5), 130.2 (C2', C6'), 134.7 (C7), 135.0 (C3', C5'), 140.0 (C4'), 155.8 (C8a), 160.8 (C2), 174.8 (C4), 187.8 (COS). MS/EI *m/z* (%): 296 (M^+, 7), 173 (100), 121 (25).

B) Synthesis of *N*-(4'-aminophenyl)-4-oxo-4*H*-chromene-3-carboxamide (10).

To a solution of compound **12** (296 mg, 0.77 mmol) in dichloromethane (12 mL) trifluoroacetic acid (TFA) (2 mL) was added. After stirred 2 hours at room temperature,

the mixture was neutralized and washed with saturated $NaHCO_3$ solution. The organic phase was dried, filtered and evaporated. The compound was obtained in 80% yield and recrystallized from CH_2Cl_2/*n*-hexane: mp 222−225 **°C.** ^{1}H NMR ($CDCl_3$) δ = 3.62 (2H, *s*, NH_2), 6.75 – 6.66 (2H, *m*, H3', H5'), 7.56 – 7.47 (3H, *m*, H2', H6', H6), 7.59 (1H, *dd*, J = 8.5, 0.6 Hz, H8), 7.78 (1H, *ddd*, J = 8.7, 7.2, 1.7 Hz, H7), 8.33 (1H, *dd*, J = 8.0, 1.5 Hz, H5), 9.06 (1H, *s*, H2), 11.18 (1H, *s*, NH). ^{13}C NMR ($CDCl_3$) δ = 115.6 (C3', C5'), 116.3 (C3), 118.7 (C8), 122.3 (C2', C6'), 124.3 (C4a), 126.4 (C6), 126.5 (C5), 129.7 (C1'), 134.9 (C7), 143.5 (C4'), 156.3 (C8a), 160.3 (CONH), 162.7 (C2), 177.6 (C4). MS/EI *m/z* (%): 281 (M^++1, 57), 280 (M^+, 100), 173 (94), 121 (64), 107 (65).

C) Synthesis of 4'-methyl-*N*-(4-oxo-4*H*-chromen-3-yl)benzamide (34).

5-(2-Hydroxyethyl)-3,4-dimethylthiazolium iodide (94 mg, 0.62 mmol) and DBU (174 µL, 0.62 mmol) were added to a solution of 2-(cyanomethoxy)benzaldehyde (500 mg, 3.1 mmol) in anhydrous dichloromethane (30 mL) and under inert atmosphere. The reaction was stirred for 5 h. Then, DIPEA (2.1 mL, 12.4 mmol) was added followed by a solution of 4-methylbenzoic acid (422 mg, 3.1 mmol) and $POCl_3$ (289 µL, 3.1 mmol) in DMF (5 mL). After 2 hours, the solution was washed with H_2O (2 x 20 mL) and saturated with a $NaHCO_3$ solution (2 x 20 mL). The organic phase was dried, filtered, and evaporated. The residue was purified by flash chromatography (CH_2Cl_2/*n*-hexane 8:2). The compound was obtained in 13% yield and recrystallized from CH_2Cl_2/*n*-hexane: mp 203−206 **°C.** ^{1}H NMR ($CDCl_3$) δ = 2.44 (3H, *s*, CH_3), 7.34 – 7.28 (2H, *m*, C3', C5'), 7.44 (1H, *ddd*, J = 8.1, 7.1, 1.0 Hz, H6), 7.55 (1H, *dd*, J = 8.5, 0.5 Hz, H8), 7.72 (1H, *ddd*, J = 8.7, 7.1, 1.7 Hz, H7), 7.88 – 7.79 (2H, *m*, H2', H6'), 8.29 (1H, *dd*, J = 8.0, 1.6 Hz, H5), 8.84 (1H, *s*, NH), 9.58 (1H, *s*, H2). ^{13}C NMR ($CDCl_3$) δ = 21.7 (CH_3), 118.7 (C8), 122.0 (C3), 124.9 (C4a), 125.0 (C6), 126.0 (C5), 127.4 (C2', C4'),

129.7 (C3', C4'), 130.9 (C1'), 134.1 (C7), 143.0 (C4'), 145.2 (C2), 156.0 (C8a), 165.6 (CONH), 172.2 (C4). MS/EI *m/z* (%): 279 (M^+, 59), 118 (100), 91 (25).

D) Synthesis of 3-((*p*-tolylamino)methyl)-4*H*-chromen-4-one (36).

To a solution of 3-formylchromone (**35**, 250 mg, 1.4 mmol) in dichloromethane (5 mL) *p*-toluidine (154 mg, 1.4 mmol) and $Na(AcO)_3BH$ (426 mg, 2 mmol) were added under inert atmosphere at room temperature. After 15 minutes, the mixture was diluted with CH_2Cl_2 (40 mL) and washed with saturated $NaHCO_3$ solution (2 x 10 mL). The organic phase was dried, filtered and evaporated. The residue was purified by flash chromatography (CH_2Cl_2). The compound was obtained in 61% yield and recrystallized from CH_2Cl_2: mp 165−168 °C. ^{1}H NMR ($CDCl_3$) δ = 2.25 (3H, *s*, CH_3), 4.28 (2H, *d*, J = 1.0 Hz, CH_2), 6.71 – 6.64 (2H, *m*, H2', H6'), 7.04 – 6.99 (2H, *m*, H3', H5'), 7.47 – 7.40 (2H, *m*, H6, H8), 7.68 (1H, *ddd*, J = 8.6, 7.1, 1.7 Hz, H7), 7.96 (1H, *t*, J = 1.0 Hz, H2), 8.25 (1H, *ddd*, J = 8.0, 1.7, 0.4 Hz, H5). ^{13}C NMR ($CDCl_3$) δ = 20.6 (CH_3), 41.5 (CH_2), 114.4 (C2', C6'), 118.3 (C8), 121.0 (C3), 123.9 (C4a), 125.3 (C6), 125.8 (C5), 128.4 (C4'), 130.0 (C3', C5'), 133.9 (C7), 144.4 (C1'), 153.6 (C2), 156.7 (C8a), 178.2 (C4). EI/ME *m/z* (%): 266 (M^++1, 138), 265 (M^+, 100), 160 (25), 120 (76), 106 (58).

E) Synthesis of (*E*)-4-oxo-4*H*-chromen-3-acrylic acid (37).

A mixture of 3-formylchromone (**35**, 1 mmol) and malonic acid (2 mmol) in the presence of pyridine (5 mL) was refluxed for 45 min with vigorous stirring. Upon completion, the mixture was cooled to room temperature, the pH adjusted to 1.0 with concentrated HCl and the reaction was stirred for additional 30 min. The yellow colored solid was filtered, washed with 1 M HCl (2 x 20 mL) and dried. The compound was obtained in 93% yield and recrystallized from MeOH: mp 156−158 °C. ^{1}H NMR

(DMSO-*d6*) δ: 7.13 (1H, *d*, J = 16 Hz, H_α), 7.44 (1H, *d*, J = 16 Hz, H_β), 7.56 (1H, *ddd*, J = 7.4, 7.2, 0.8 Hz, H6), 7.71 (1H, *dd*, J = 8.8, 0.4 Hz, H8), 7.85 (1H, *ddd*, J = 7.4, 7.2, 0.8 Hz, H7), 8.14 (1H, *dd*, J = 8.8, 0.4 Hz, H5), 8.88 (1H, *s*, H2). ^{13}C NMR (DMSO-*d6*) δ: 118.2 (C8), 118.6 (C3), 121.4 (C4a), 123.6 (C_α), 125.5 (C6), 126.2 (C5), 134.7 (C7), 136.0 (C_β), 155.2 (C8a), 159.9 (C2), 167.8 (COOH), 175.3 (CO). MS/EI *m/z* (%): 266 (M^+, 8), 171 (100).

F) Synthesis of chromone carboxamides with a vinylic spacer (38-41).

Compound **37** (250 mg, 1.31 mmol) was dissolved in DMF (6 mL) and DIPEA (0.190 mL). The solution was cooled at 0 ºC and a solution of PyBOP (580 mg, 1.31 mmol) in CH_2Cl_2 (6 mL) was added. The mixture was stirred during 30 min. Then, the amine with the desired aromatic pattern (phenylamine, 4-methylphenylamine, 4-chlorophenylamine or 3,4-dimethylphenylamine) (1.31 mmol) was added. The temperature was gradually increased to room temperature and the reaction kept under stirring for another 6 h. The mixture was then diluted with ethyl acetate (20 mL), washed with H_2O (2 x 20 mL) and HCl 1 M. The organic phase was dried, filtered and evaporated. The residues were purified by flash chromatography (CH_2Cl_2/diethyl ether) and/or crystallization from ethyl acetate.

(*E*)-*N*-Phenyl-4-oxo-4*H*-chromen-3-acrylamide (38). The compound was obtained in 11% yield and recrystallized from AcOEt: mp 235−238 **°C.** ^{1}H NMR (DMSO-*d6*) δ: 7.09-7.03 (1H, *m*, H4'), 7.35-7.30 (2H, *m*, H3', H5'), 7.40 (1H, *dd*, J = 15.6 Hz, H_β), 7.56 (1H, *m*, H6), 7.66 (1H, *d*, J = 15.6 Hz, H_α), 7.76-7.70 (3H, *m*, H8, H2', H6'), 7.86 (1H, *ddd*, J = 7.8, 7.0, 1.6 Hz, H7), 8.18 (1H, *dd*, J = 8.0, 1.2 Hz, H5), 8.86 (1H, *s*, H2), 10.45 (1H, *s*, NH). ^{13}C NMR (DMSO-*d6*) δ: 118.9 (C8), 119.0 (C3), 119.7 (C2', C6'),

123.8 (C_α), 124.0 (C4a), 125.5 (C6), 125.9 (C5), 126.5 (C4'), 129.2 (C3', C5'), 132.9 (C7), 134.9 (C_β), 139.9 (C1'), 155.5 (C8a), 160.4 (C7'), 164.6 (C2), 176.0 (C4). MS/EI *m/z* (%): 291 (M^+, 73), 199 (100), 172 (22), 171 (100), 115 (21), 93 (24), 51 (20).

(*E*)-*N*-(4'-Chlorophenyl)-4-oxo-4*H*-chromen-3-acrylamide (39). The compound was obtained in 15% yield and recrystallized from AcOEt: mp 260−263 **°C.** ^{1}H NMR (DMSO-*d6*) δ: 7.43-7.36 (3H, *m*, H_β, H3', H5'), 7.56 (1H, *ddd*, J = 7.6, 7.2, 1.6 Hz, H6), 7.66 (1H, *d*, J = 15.6 Hz, H_α), 7.72 (1H, *dd*, J = 8.4, 0.4 Hz, H8), 7.76 (2H, *dt*, J = 9.2, 2.6, 2.4 Hz, H2', H6'), 7.86 (1H, *ddd*, J = 7.6, 7.2, 1.6 Hz, H7), 8.18 (1H, *dd*, J = 8.4, 0.4 Hz, H5), 8.86 (1H, *s*, H2), 10.45 (1H, *s*, NH). ^{13}C NMR (DMSO-d6) δ: 119.0 (C3), 119.9 (C8), 121.2 (C2', C6'), 124.0 (C4a), 125.1 (C_α), 125.9 (C6), 126.5 (C5), 127.3 (C4'), 129.1 (C3', C5'), 133.3 (C7), 135.0 (C_β), 138.8 (C1'), 155.5 (C8a), 160.6 (7'), 164.7 (C2), 176.0 (C4). MS/EI *m/z* (%): 327 (M^++2, 26), 325 (M^+, 69), 200 (68), 199 (100), 172 (33), 171 (100), 127 (21), 121 (20) 115 (35), 79 (28), 51 (30).

(*E*)-*N*-(*p*-Tolyl)-4-oxo-4H-chromen-3-acrylamide (40). The compound was obtained in 26% yield and recrystallized from AcOEt: mp 193−197 **°C.** ^{1}H NMR (DMSO-*d6*) δ: 2.26 (3H, *s*, CH_3), 7.12 (2H, *d*, *J* = 8.4 Hz, H3', H5'), 7.37 (1H, *dd*, J = 0.4, 15.6 Hz, H_β), 7.56 (1H, *ddd*, J = 7.6, 7.2, 1.6 Hz H6), 7.67-7.59 (3H, *m*, H_α, H2', H6'), 7.64 7.72 (1H, *dd*, J = 8.4, 0.8 Hz, H8), 7.86 (1H, *ddd*, J = 7.6, 7.2, 1.6 Hz Hz, H7), 8.17 (1H, *dd*, J = 8.0, 0.8 Hz, H5), 8.84 (1H, *s*, H2), 10.22 (1H, *s*, NH). ^{13}C NMR (DMSO-*d6*) δ: 119.0 (C8), 119.1 (C3), 119.7 (C2', C6'), 124.0 (C4a), 125.6 (C_α), 125.9 (C6), 126.4 (C5), 129.6 (C3', C5'), 132.4 (C7), 132.6 (C4'), 134.9 (C_β), 137.4 (C1'), 155.5 (C8a), 160.3 (C7'), 164.3 (C2), 175.9 (C4). MS/EI *m/z* (%): 306 (M^++1, 39), 305 (M^+, 98), 200 (48), 199 (97), 172 (38), 171 (100), 115 (21), 107 (38).

(*E*)-*N*-(3',4'-Dimethylphenyl)-4-oxo-4*H*-chromen-3-acrylamide (41). The compound was obtained in 18% yield and recrystallized from AcOEt: mp 197−200 **°C.** ^{1}H NMR (DMSO-*d6*) δ: 2.18 (3H, *s*, C$\underline{H}_3$), 2.20 (3H, *s*, C$\underline{H}_3$), 7.06 (1H, *d*, J = 8 Hz, H2'), 7.35 (1H, *dd*, J = 15.6 Hz, H_β), 7.50-7.44 (2H, *m*, H5', H6'), 7.55 (1H, *ddd*, J = 7.6, 7.2, 1.2 Hz, H6), 7.63 (1H, *d*, J = 15.6 Hz, H_α), 7.72 (1H, *dd*, J = 8.4, 0.8 Hz, H8), 7.85 (1H, *ddd*, J = 7.6, 7.2, 1.2 Hz, H7), 8.17 (1H, *dd*, J = 8.0, 0.8 Hz, H5), 8.83 (1H, *s*, H2), 10.14 (1H, *s*, N$\underline{H}$). ^{13}C NMR (DMSO-*d6)* δ: 19.3 (CH_3), 20.1 (CH_3), 117.3 (C8), 119.0 (C6'), 119.2 (C3), 120.9 (C2'), 124.0 (C4a), 125.7 (C_α), 125.9 (C6), 126.4 (C5), 130.0 (C5'), 131.5 (C4'), 132.4 (C7), 134.9 (C_β), 136.7 (C3'), 137.6 (C1'), 155.5 (C8a), 160.2 (C7'), 164.3 (C2), 175.9 (C4). MS/EI *m/z* (%): 319 (M^+, 45), 199 (100), 171 (81), 121 (29).

Pharmacology.

Evaluation of monoamine oxidase (hMAOs)inhibitiory activity. The inhibitory activity of the chromones under study on both *h*MAO isoforms was assessed following a previously described method.[10]

Briefly, the inhibitory activity on *h*MAOs was evaluated by measuring the effects of the chromones on the production of hydrogen peroxide (H_2O_2) from p-tyramine, using the Amplex Red MAO assay kit (Molecular Probes, Inc., Eugene, OR, U.S.) and microsomal MAO isoforms prepared from insect cells (BTI-TN-5B1-4) infected with recombinant baculovirus containing cDNA inserts for *h*MAO-A or *h*MAO-B (Sigma-Aldrich Química S.A). The test compounds/ standard inhibitors and adequate amounts of recombinant *h*MAO-A or *h*MAO-B were incubated for 15 min at 37˚C in a flat-black-bottom 96-well microplate (BRANDplates, pureGradeTM, BRAND GMBH,

Wertheim, Germany) with Amplex Red® reagent, 1 U/mL horseradish peroxidase, and 1 mM *p*-tyramine. The production of H_2O_2 and consequently of resorufin was quantified at 37˚C in a multimode microplate reader (Biotek Synergy HT), based on the fluorescence generated (excitation, 545 nm, emission, 590 nm) over a 15 min period, in which the fluorescence increased linearly. Control experiments were carried out simultaneously by replacing the test drugs (new compounds and standard inhibitors) with appropriate dilutions of the vehicles. The IC_{50} values were determined in triplicate from the dose-response inhibition curves and are expressed as mean ± standard deviation (SD). All IC_{50} values are the mean ± S.D. from three experiments.

Evaluation of hMAO-A and hMAO-B kinetics. To determine the steady-state kinetic parameters (K_m, Michaelis constant and V_{max}, maximum rate) of *h*MAO-A and *h*MAO-B the enzymatic activity of both isoforms was evaluated (under the experimental conditions described above) in the presence of different p-tyramine concentrations. Under our experimental conditions, hMAO-A displayed a K_m of 449.08 ± 28.42 μM and a V_{max} of 30.03 ± 0.6529 nmol/min whereas hMAO-B showed a K_m of 58.76 ± 11.67 μM and a V_{max} of 22.60 ± 1.018 nmol/min (n=3).

Evaluation of hMAO-B-inhibitor kinetics. To evaluate the mechanism of *h*MAO-B inhibition of the most promising chromones (**20** and **27**) substrate-dependent kinetic experiments were performed. The catalytic rates of *h*MAO-B were measured at five different concentrations of p-tyramine substrate (0.031 – 2 mM) in the absence or presence of the selected inhibitors (compounds **20** and **27**) and standard inhibitors, at concentrations between 0.5 and 1.0 nM. The results are presented as double reciprocal Lineweaver-Burk plots (1/V vs. 1/[S]) and the kinetic data, namely Michaelis-Menten

constant (K_m) and maximum reaction rate (V_{max}), was acquired employing Michaelis-Menten equation. The Ki values were estimated using Dixon plots, by replotting the slope of each Lineweaver-Burk plot versus the inhibitor concentration. In the Dixon plots, the Ki valued were obtained from the x-axis intercept ($-K_i$). The enzymatic reactions and measurements were performed using the same *h*MAO-B assay conditions as described above (n=3). Linear regression analysis was performed using Prism 5.

Evaluation of hMAO-B-inhibitior type of binding affinity. The analysis of the type of binding of chromones **20** and **27** and the standard inhibitors with *h*MAO-B was performed by a time-dependent inhibition assay. The enzyme was incubated for a 60 minute period with the chromone based inhibitors as well as the standard inhibitors at their IC_{80} values. The final well concentrations were: compound **20** (0.7 nM), compound **27** (2 nM), (R)-(−)-deprenyl (50 nM), safinamide (40 nM) and rasagiline (200 nM) and MAO-B (6.4 μg/mL). Control experiments without inhibitors were run simultaneously. The enzymatic activity was determined as described above (see determination of *h*MAO isoform activity). The percentage of enzyme activity was plotted against the incubation time to determine time-dependent enzyme-inhibition. Data are the mean ± SD of three independent experiments.

Evaluation of cytotoxicity for the most active compounds

Reagents. (4,5-dimethylthiazol-2-yl)-2,5-diphenyl tetrazolium (MTT) bromide and Dulbecco's modified Eagle's medium (DMEM) with 4.5 g/L glucose were obtained from Sigma (St. Louis, MO, USA). Reagents used in cell culture, including nonessential amino acids (NEAA), heat inactivated fetal bovine serum (FBS), 0.05% trypsin/1 mM EDTA, antibiotic (10000 U/mL penicillin, 10000 μg/mL streptomycin), phosphate-

buffered saline solution (PBS) and Hank's balanced salt solution (HBSS) were purchased from Gibco Laboratories (Lenexa, KS). Dimethylsulfoxide (DMSO-*d6*), absolute ethanol and acetic acid were obtained from Merck (Darmstadt, Germany). All reagents were of analytical grade or of the highest grade available.

Cell culture. SH-SY5Y cells (ATCC, Manassas, VA, USA), a neuroblastoma cell line, were routinely cultured in 75-cm2 flasks (Corning Costar, Corning, NY, USA) using DMEM with 4.5 g/L glucose, supplemented with 10 % heat-inactivated FBS (v/v), 1 % NEAA (v/v), 100 U/mL penicillin, and 100 μg/mL streptomycin. Cells were maintained at 37 °C in a humidified atmosphere of 95 % air/5 % CO2 and the medium was changed every 2 days. The cells used for all the experiments were taken between the 25th and 34th passages, in order to avoid phenotypic changes. Cultures were passaged weekly by trypsinization (0.05% trypsin/1 mM EDTA). For the cytotoxicity experiments, undifferentiated SH-SY5Y cells were seeded onto 96-well plates (25000 cells/cm2) in complete cell culture medium, and cultured for 3 days at 37 °C. Three days after seeding, when confluence was reached, the cells were exposed to the test compounds (0, 1, and 50.0 μM) in cell culture medium without FBS for 24 h. Cytotoxicity was evaluated 24 h after exposure, by the MTT reduction and by the NR uptake assays.

MTT reduction assay. The MTT reduction assay was used to measure mitochondrial dysfunction (decrease in mitochondrial dehydrogenase activity) in cells exposed to the test compounds. The signal generated is dependent on the degree of reduction of the MTT tetrazolium salt (water soluble) to MTT formazan (water insoluble) by cellular dehydrogenases within metabolically active cells. At the selected time point, the cell culture medium was removed, followed by the addition of fresh cell culture medium containing 0.5 mg/mL MTT and incubation at 37 °C in a humidified, 5% CO2 atmosphere for 2 h. After this incubation period, the cell culture medium was removed

and the formed formazan crystals dissolved in 100% DMSO. The absorbance was measured at 550 nm in a multi-well plate reader (BioTek Instruments, Vermont, USA). The percentage of MTT reduction relative to that of the control cells was used as the cytotoxicity measure [MTT reduction (% of control)].

Neutral red uptake assay. The NR uptake assay is based on the ability of viable cells to incorporate and bind the supravital dye neutral red in the lysosomes, thus providing a quantitative estimation of the number of viable cells in a culture. Twenty-four hours after exposure, the cell culture medium was removed and the cells incubated with neutral red (50 μg/mL in cell culture medium) at 37 °C, in a humidified, 5% CO2-95% air atmosphere, for 2 h. After this incubation period, the cell culture medium was removed, the dye absorbed only by viable cells extracted [with absolute ethyl alcohol /distilled water (1:1) containing 5% acetic acid], and the absorbance measured at 540 nm in a multi-well plate reader (BioTek Instruments, Vermont, USA). The percentage of NR uptake relative to that of the control cells was used as the cytotoxicity measure [NR uptake (% of control)].

Data analysis

For the enzymatic inhibition studies, the compounds were initially screened at 10 μM. For potent compounds, dose-response curves were plotted and IC50 values were estimated by non-linear analysis. For the cytotoxicity assays, MTT reduction for each treatment as calculated as the % of control untreated cells and plotted in column graphs. Statistical comparisons between groups were carried by one-way analysis of variance (ANOVA-1) followed by Dunnett comparison post-test ($\alpha = 0.05$, 95 % confidence intervals). Differences were considered to be significant for p values lower than 0.05. All plots and statistical analysis were performed using GraphPad Prism 5 Software.

Molecular modelling. *h*MAO-A and *h*MAO-B receptor models were built following the a consolidated procedure previously reported,[29] i.e. starting from the Protein Data Bank (PDB)[30] deposited crystallographic structures 2Z5X[31] and 2V5Z[8], respectively. Both experimental structures were submitted to a preliminary pre-treatment: a) the co-crystallised reversible ligands, harmine for 2Z5X and safinamide for 2V5Z, and water molecules were removed, b) FAD cofactor bonds order was fixed and hydrogen atoms were added. Modified structures were submitted to protein heavy atoms 50 kJ/mol·Å constrained energy minimisation using 10,000 steps of the Polak Ribiere Conjugate Gradient algorithm, as implemented in MacroModel program.[32] Optimised receptor models were considered for mimicking *h*MAO-A and *h*MAO-B and, in both cases, the ligand binding site was represented by an N5 FAD atom centred regular box of 27,000 Å^3. Inhibitor chemical structures were built and optimised using the Maestro GUI.[33] Docking simulations were carried out using the standard precision (SP) search algorithms of Glide software.[34] Ligands structural flexibility was taken into account by means of the corresponding software implementation. A maximum of 10 docking configuration were sampled. Default Glide scoring function (GScore) was applied for poses ranking (Table S1). Further analysis and simulation were carried out on compounds **20** and **27** MAOs complexes taking into account both the absolutely docking GScore top ranked configuration (TC) and the relative top ranked configuration reporting opposite orientation with respect to TC (SC). For both targets, ligand free (LF), TC and SC models were explicitly solvated with water molecules included by the Impact[35] "Soak" method. For all structures a regular box, of 64,000 Å^3 centred onto the N5 FAD atom, was considered for the solvent positioning (Table S2). The resulting structures were submitted for Molecular Dynamics (MD) simulation carried out using

the Desmond software.[36] The SPC explicit solvent model was applied for generating solvated MD suitable systems. The overall electrostatic net charge of the starting structures was neutralized including 3 Cl^- ions into the *h*MAO-A models and 3 Na^+ ions into the *h*MAO-B ones. The default Desmond protocol was applied for equilibrating solvated systems. The production MD simulation was carried out at 300 °K, up to 1.2 ns, using an integration time step equal to 2 fs. MD frames were sampled at regular time intervals equal to 10 ps. The targets structural perturbation induced by our inhibitors recognition was evaluated by computing the root mean square deviation (RMSd) of TC and SC MD trajectories with respect to the corresponding LF ones. The RMSd data were computed taking into account the targets not hydrogen atoms.

ASSOCIATED CONTENT

Supporting Information Available

Additional molecular docking data was included in supporting information that is available free of charge on ACS Publications website.

Molecular formula strings (CSV)

AUTHOR INFORMATION

Corresponding Author

Fernanda Borges, CIQUP/Department of Chemistry and Biochemistry, Faculty of Sciences, University of Porto, Porto 4169-007, Portugal. Phone*: +351 220402560. E-mail: fborges@fc.up.pt*

Author Contributions

[¥]Joana Reis, Fernando Cagide and Francesco Ortuso contributed equally.

Notes

The authors declare no competing financial interest.

ACKOWLEDGEMENTS

This project was supported by Foundation for Science and Technology (FCT) and FEDER/COMPETE2020 (UID/QUI/00081/2015 and POCI-01-0145-FEDER-006980). The authors also thank the COST action CA15135 (Multi-target paradigm for innovative ligand identification in the drug discovery process MuTaLig) for support.

J. Reis (SFRH/BD/96033/2013), F. Cagide (SFRH/BPD/74491/2010), D. Chavarria (SFRH/BD/108119/2015), T. Silva (SFRH/BD/79671/2011), C Fernandes (SFRH/BD/98519/2013) and A. Gaspar (SFRH/BPD/93331/2013) grants are also supported by FCT and FEDER/COMPETE funds.

ABBREVIATIONS

AEI, ADMET efficiency index; DIPEA, *N,N*-Diisopropylethylamine; IMAO-B; monoamine oxidase-B inhibitors; LE, ligand efficiency; LLE, lipophilic ligand efficiency; log BB, blood (plasma)-brain partitioning; MAO, monoamine oxidase; *h*MAO-A, human monoamine oxidase A; *h*MAO-B, human monoamine oxidase B; MD, molecular dynamics; MTT, 3-(4,5-dimethylthiazol-2-yl)-2,5-diphenyltetrazolium bromide; NR, 3-amino-7-dimethylamino-2-methylphenazine hydrochloride; PD, Parkinson's disease; PyBOP, benzotriazol-1-yloxy)-tripyrrolidinophosphonium hexafluorophosphate; SI, selectivity index; tPSA, topological polar surface area.

REFERENCES

1. Jankovic, J.; Aguilar, L. G. Current approaches to the treatment of Parkinson's disease. *Neuropsychiatr. Dis. Treat.* **2008,** *4*, 743-757.

2. Schapira, A. H. V. Present and future drug treatment for Parkinson's disease. *J. Neurol. Neurosurg. Psychiatry* **2005,** *76*, 1472-1478.

3. Keith, F. T.; Sinead, B.; Jeff, O.; Sullivan; Gavin, P. D.; Joe, H. Monoamine oxidases: certainties and uncertainties. *Curr. Med. Chem.* **2004,** *11*, 1965-1982.

4. Youdim, M. B.; Bakhle, Y. S. Monoamine oxidase: isoforms and inhibitors in Parkinson's disease and depressive illness. *Br. J. Pharmacol.* **2006,** *147 Suppl 1*, S287-296.

5. Youdim, M. B. H. Why do we need multifunctional neuroprotective and neurorestorative drugs for Parkinson's and Alzheimer's diseases as disease modifying agents. *Exp. Neurobiol.* **2010,** *19*, 1-14.

6. De la Fuente-Fernández, R.; Sossi, V.; Huang, Z.; Furtado, S.; Lu, J.-Q.; Calne, D. B.; Ruth, T. J.; Stoessl, A. J. Levodopa-induced changes in synaptic dopamine levels increase with progression of Parkinson's disease: implications for dyskinesias. *Brain* **2004,** *127*, 2747-2754.

7. Youdim, M. B. H.; Gross, A.; Finberg, J. P. M. Rasagiline [N-propargyl-1R(+)-aminoindan], a selective and potent inhibitor of mitochondrial monoamine oxidase B. *Br. J. Pharmacol.* **2001,** *132*, 500-506.

8. Binda, C.; Wang, J.; Pisani, L.; Caccia, C.; Carotti, A.; Salvati, P.; Edmondson, D. E.; Mattevi, A. Structures of human monoamine oxidase B complexes with selective noncovalent inhibitors: safinamide and coumarin analogs. *J. Med. Chem.* **2007,** *50*, 5848-5852.

9. Ellis, G. P. *The Chemistry of Heterocyclic Compounds, Chromenes, Chromanones, and Chromones*. Wiley: New York, 2009; Vol. 31, p 1085.

10. Gaspar, A.; Matos, M. J.; Garrido, J.; Uriarte, E.; Borges, F. Chromone: a valid scaffold in medicinal chemistry. *Chem. Rev.* **2014,** *114*, 4960-4992.

11. Alcaro, S.; Gaspar, A.; Ortuso, F.; Milhazes, N.; Orallo, F.; Uriarte, E.; Yáñez, M.; Borges, F. Chromone-2- and -3-carboxylic acids inhibit differently monoamine oxidases A and B. *Bioorg. Med. Chem. Lett.* **2010,** *20*, 2709-2712.

12. Gaspar, A.; Reis, J.; Fonseca, A.; Milhazes, N.; Viña, D.; Uriarte, E.; Borges, F. Chromone 3-phenylcarboxamides as potent and selective MAO-B inhibitors. *Bioorg. Med. Chem. Lett.* **2011,** *21*, 707-709.

13. Gaspar, A.; Teixeira, F.; Uriarte, E.; Milhazes, N.; Melo, A.; Cordeiro, M. N. D. S.; Ortuso, F.; Alcaro, S.; Borges, F. Towards the discovery of a novel class of monoamine oxidase inhibitors: structure–property–activity and docking studies on chromone amides. *ChemMedChem* **2011,** *6*, 628-632.

14. Gaspar, A.; Silva, T.; Yáñez, M.; Vina, D.; Orallo, F.; Ortuso, F.; Uriarte, E.; Alcaro, S.; Borges, F. Chromone, a privileged scaffold for the development of monoamine oxidase inhibitors. *J. Med. Chem.* **2011,** *54*, 5165-5173.

15. Cagide, F.; Silva, T.; Reis, J.; Gaspar, A.; Borges, F.; Gomes, L. R.; Low, J. N. Discovery of two new classes of potent monoamine oxidase-B inhibitors by tricky chemistry. *Chem. Commun.* **2015,** *51*, 2832-2835.

16. Cagide, F.; Reis, J.; Gaspar, A.; Borges, F. Accelerating lead optimization of chromone carboxamide scaffold throughout microwave-assisted organic synthesis. *Tetrahedron Lett.* **2011,** *52*, 6446-6449.

17. Vedachalam, S.; Zeng, J.; Gorityala, B. K.; Antonio, M.; Liu, X.-W. N-Heterocyclic carbene-catalyzed intramolecular aldehyde−nitrile cross coupling: an easy access to 3-aminochromones. *Org. Lett.* **2010,** *12*, 352-355.

18. Abdel-Magid, A. F.; Carson, K. G.; Harris, B. D.; Maryanoff, C. A.; Shah, R. D. Reductive amination of aldehydes and ketones with sodium triacetoxyborohydride. Studies on direct and indirect reductive amination procedures. *J. Org. Chem.* **1996,** *61*, 3849-3862.

19. Joshi, R. S.; Mandhane, P. G.; Badadhe, P. V.; Gill, C. H., Development of practical methodologies for the synthesis of novel 3(4-oxo-4*H*-chromen-3-yl)acrylic acid hydrazides. *Ultrason. Sonochem.* **2011,** *18*, 735-738.

20. Gaspar, A.; Reis, J.; Matos, M. J.; Uriarte, E.; Borges, F. In search for new chemical entities as adenosine receptor ligands: development of agents based on benzo-*γ*-pyrone skeleton. *Eur. J. Med. Chem.* **2012,** *54*, 914-918.

21. Leeson, P. D.; Springthorpe, B. The influence of drug-like concepts on decision-making in medicinal chemistry. *Nat. Rev. Drug Discovery* **2007,** *6*, 881-890.

22. Clark, D. E. Rapid calculation of polar molecular surface area and its application to the prediction of transport phenomena. 2. Prediction of blood-brain barrier penetration. *J. Pharm. Sci.* **1999,** *88*, 815-821.

23. Barton, P.; Riley, R. J. A new paradigm for navigating compound property related drug attrition. *Drug Discovery Today* **2016,** *21*, 72-81.

24. Lipinski, C. A.; Lombardo, F.; Dominy, B. W.; Feeney, P. J. Experimental and computational approaches to estimate solubility and permeability in drug discovery and development settings. *Adv. Drug Delivery Rev.* **2001,** *46*, 3-26.

25. Hitchcock, S. A.; Pennington, L. D. Structure−brain exposure relationships. *J. Med. Chem.* **2006,** *49*, 7559-7583.

26. Pajouhesh, H.; Lenz, G. R. Medicinal chemical properties of successful central nervous system drugs. *NeuroRx* **2005,** *2*, 541-553.

27. Baell, J. B.; Holloway, G. A. New substructure filters for removal of pan assay interference compounds (PAINS) from screening libraries and for their exclusion in bioassays. *J. Med. Chem.* **2010**, *53*, 2719–2740.

28. Lobner, D. Comparison of the LDH and MTT assays for quantifying cell death: validity for neuronal apoptosis? *J. Neurosci. Methods* **2000,** *96*, 147-152.

29. Chimenti, F.; Bolasco, A.; Secci, D.; Chimenti, P.; Granese, A.; Carradori, S.; Yanez, M.; Orallo, F.; Ortuso, F.; Alcaro, S. Investigations on the 2-thiazolylhydrazyne scaffold: synthesis and molecular modeling of selective human monoamine oxidase inhibitors. *Bioorg. Med. Chem.* **2010,** *18*, 5715-5723.

30. Berman, H. M.; Westbrook, J.; Feng, Z.; Gilliland, G.; Bhat, T. N.; Weissig, H.; Shindyalov, I. N.; Bourne, P. E. The Protein Data Bank. *Nucleic Acids Res.* **2000,** *28*, 235-242.

31. Son, S. Y.; Ma, J.; Kondou, Y.; Yoshimura, M.; Yamashita, E.; Tsukihara, T. Structure of human monoamine oxidase A at 2.2-A resolution: the control of opening the entry for substrates/inhibitors. *Proc. Natl. Acad. Sci. U S A* **2008,** *105*, 5739-5744.

32. *MacroModel,* version 10.8, Schrödinger, LLC, New York, NY, 2015

33. *Maestro*, version 10.2, Schrödinger, LLC, New York, NY, 2015

34. *Glide*, version 6.7, Schrödinger, LLC, New York, NY, 2015

35. *Impact*, version 6.7, Schrödinger, LLC, New York, NY, 2015

36. *Desmond Molecular Dynamics System*, version 4.2, D. E. Shaw Research, New York, NY, 2015

Table of Contents Graphic

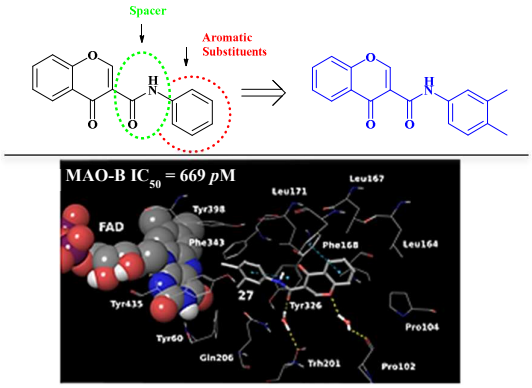

Table of Contents Graphic

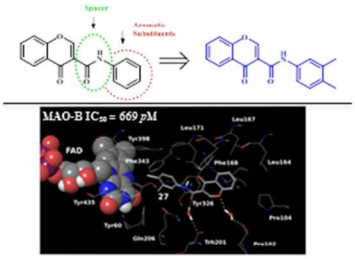

190x254mm (96 x 96 DPI)